Higgs boson searches in CP-conserving and CP-violating MSSM scenarios with the DELPHI detector

DELPHI Collaboration

Abstract

This paper presents the final interpretation of the results from DELPHI on the searches for Higgs bosons in the Minimal Supersymmetric extension of the Standard Model (MSSM). A few representative scenarios are considered, that include CP conservation and explicit CP violation in the Higgs sector. The experimental results encompass the searches for neutral Higgs bosons at LEP1 and LEP2 in final states as expected in the MSSM, as well as LEP2 searches for charged Higgs bosons and for neutral Higgs bosons decaying into hadrons independent of the quark flavour. The data reveal no significant excess with respect to background expectations. The results are translated into excluded regions of the parameter space in the various scenarios. In the CP-conserving case, these lead to limits on the masses of the lightest scalar and pseudoscalar Higgs bosons, h and A, and on $\tan\beta$. The dependence of these limits on the top quark mass is discussed. Allowing for CP violation reduces the experimental sensitivity to Higgs bosons. It is shown that this effect depends strongly on the values of the parameters responsible for CP violation in the Higgs sector.

J.Abdallah[26], P.Abreu[23], W.Adam[55], P.Adzic[12], T.Albrecht[18], R.Alemany-Fernandez[9], T.Allmendinger[18], P.P.Allport[24], U.Amaldi[30], N.Amapane[48], S.Amato[52], E.Anashkin[37], A.Andreazza[29], S.Andringa[23], N.Anjos[23], P.Antilogus[26], W-D.Apel[18], Y.Arnoud[15], S.Ask[27], B.Asman[47], J.E.Augustin[26], A.Augustinus[9], P.Baillon[9], A.Ballestrero[49], P.Bambade[21], R.Barbier[28], D.Bardin[17], G.J.Barker[57], A.Baroncelli[40], M.Battaglia[9], M.Baubillier[26], K-H.Becks[58], M.Begalli[7], A.Behrmann[58], E.Ben-Haim[21], N.Benekos[33], A.Benvenuti[5], C.Berat[15], M.Berggren[26], L.Berntzon[47], D.Bertrand[2], M.Besancon[41], N.Besson[41], D.Bloch[10], M.Blom[32], M.Bluj[56], M.Bonesini[30], M.Boonekamp[41], P.S.L.Booth[†24], G.Borisov[22], O.Botner[53], B.Bouquet[21], T.J.V.Bowcock[24], I.Boyko[17], M.Bracko[44], R.Brenner[53], E.Brodet[36], P.Bruckman[19], J.M.Brunet[8], B.Buschbeck[55], P.Buschmann[58], M.Calvi[30], T.Camporesi[9], V.Canale[39], F.Carena[9], N.Castro[23], F.Cavallo[5], M.Chapkin[43], Ph.Charpentier[9], P.Checchia[37], R.Chierici[9], P.Chliapnikov[43], J.Chudoba[9], S.U.Chung[9], K.Cieslik[19], P.Collins[9], R.Contri[14], G.Cosme[21], F.Cossutti[50], M.J.Costa[54], D.Crennell[38], J.Cuevas[35], J.D'Hondt[2], J.Dalmau[47], T.da Silva[52], W.Da Silva[26], G.Della Ricca[50], A.De Angelis[51], W.De Boer[18], C.De Clercq[2], B.De Lotto[51], N.De Maria[48], A.De Min[37], L.de Paula[52], L.Di Ciaccio[39], A.Di Simone[40], K.Doroba[56], J.Drees[58,9], G.Eigen[4], T.Ekelof[53], M.Ellert[53], M.Elsing[9], M.C.Espirito Santo[23], G.Fanourakis[12], D.Fassouliotis[12,3], M.Feindt[18], J.Fernandez[42], A.Ferrer[54], F.Ferro[14], U.Flagmeyer[58], H.Foeth[9], E.Fokitis[33], F.Fulda-Quenzer[21], J.Fuster[54], M.Gandelman[52], C.Garcia[54], Ph.Gavillet[9], E.Gazis[33], R.Gokieli[9,56], B.Golob[44,46], G.Gomez-Ceballos[42], P.Goncalves[23], E.Graziani[40], G.Grosdidier[21], K.Grzelak[56], J.Guy[38], C.Haag[18], A.Hallgren[53], K.Hamacher[58], K.Hamilton[36], S.Haug[34], F.Hauler[18], V.Hedberg[27], M.Hennecke[18], H.Herr[†9], J.Hoffman[56], S-O.Holmgren[47], P.J.Holt[9], M.A.Houlden[24], J.N.Jackson[24], G.Jarlskog[27], P.Jarry[41], D.Jeans[36], E.K.Johansson[47], P.D.Johansson[47], P.Jonsson[28], C.Joram[9], L.Jungermann[18], F.Kapusta[26], S.Katsanevas[28], E.Katsoufis[33], G.Kernel[44], B.P.Kersevan[44,46], U.Kerzel[18], B.T.King[24], N.J.Kjaer[9], P.Kluit[32], P.Kokkinias[12], C.Kourkoumelis[3], O.Kouznetsov[17], Z.Krumstein[17], M.Kucharczyk[19], J.Lamsa[1], G.Leder[55], F.Ledroit[15], L.Leinonen[47], R.Leitner[31], J.Lemonne[2], V.Lepeltier[21], T.Lesiak[19], W.Liebig[58], D.Liko[55], A.Lipniacka[47], J.H.Lopes[52], J.M.Lopez[35], D.Loukas[12], P.Lutz[41], L.Lyons[36], J.MacNaughton[55], A.Malek[58], S.Maltezos[33], F.Mandl[55], J.Marco[42], R.Marco[42], B.Marechal[52], M.Margoni[37], J-C.Marin[9], C.Mariotti[9], A.Markou[12], C.Martinez-Rivero[42], J.Masik[13], N.Mastroyiannopoulos[12], F.Matorras[42], C.Matteuzzi[30], F.Mazzucato[37], M.Mazzucato[37], R.Mc Nulty[24], C.Meroni[29], E.Migliore[48], W.Mitaroff[55], U.Mjoernmark[27], T.Moa[47], M.Moch[18], K.Moenig[9,11], R.Monge[14], J.Montenegro[32], D.Moraes[52], S.Moreno[23], P.Morettini[14], U.Mueller[58], K.Muenich[58], M.Mulders[32], L.Mundim[7], W.Murray[38], B.Muryn[20], G.Myatt[36], T.Myklebust[34], M.Nassiakou[12], F.Navarria[5], K.Nawrocki[56], R.Nicolaidou[41], M.Nikolenko[17,10], A.Oblakowska-Mucha[20], V.Obraztsov[43], A.Olshevski[17], A.Onofre[23], R.Orava[16], K.Osterberg[16], A.Ouraou[41], A.Oyanguren[54], M.Paganoni[30], S.Paiano[5], J.P.Palacios[24], H.Palka[19], Th.D.Papadopoulou[33], L.Pape[9], C.Parkes[25], F.Parodi[14], U.Parzefall[9], A.Passeri[40], O.Passon[58], L.Peralta[23], V.Perepelitsa[54], A.Perrotta[5], A.Petrolini[14], J.Piedra[42], L.Pieri[40], F.Pierre[41], M.Pimenta[23], E.Piotto[9], T.Podobnik[44,46], V.Poireau[9], M.E.Pol[6], G.Polok[19], V.Pozdniakov[17], N.Pukhaeva[17], A.Pullia[30], J.Rames[13], A.Read[34], P.Rebecchi[9], J.Rehn[18], D.Reid[32], R.Reinhardt[58], P.Renton[36], F.Richard[21], J.Ridky[13], M.Rivero[42], D.Rodriguez[42], A.Romero[48], P.Ronchese[37], P.Roudeau[21], T.Rovelli[5], V.Ruhlmann-Kleider[41], D.Ryabtchikov[43], A.Sadovsky[17], L.Salmi[16], J.Salt[54], C.Sander[18], A.Savoy-Navarro[26], U.Schwickerath[9], R.Sekulin[38], M.Siebel[58], A.Sisakian[17], G.Smadja[28], O.Smirnova[27], A.Sokolov[43], A.Sopczak[22], R.Sosnowski[56], T.Spassov[9], M.Stanitzki[18], J.Strauss[55], B.Stugu[4], M.Szczekowski[56], M.Szeptycka[56], T.Szumlak[20], T.Tabarelli[30], A.C.Taffard[24], F.Tegenfeldt[53], J.Timmermans[32], L.Tkatchev[17], M.Tobin[24], S.Todorovova[13], B.Tome[23], A.Tonazzo[30], P.Tortosa[54], P.Travnicek[13], D.Treille[9], G.Tristram[8], M.Trochimczuk[56], C.Troncon[29], M-L.Turluer[41], I.A.Tyapkin[17], P.Tyapkin[17], S.Tzamarias[12], V.Uvarov[43], G.Valenti[5], P.Van Dam[32], J.Van Eldik[9], N.van Remortel[16], I.Van Vulpen[9], G.Vegni[29], F.Veloso[23], W.Venus[38], P.Verdier[28], V.Verzi[39], D.Vilanova[41], L.Vitale[50], V.Vrba[13], H.Wahlen[58], A.J.Washbrook[24], C.Weiser[18], D.Wicke[9], J.Wickens[2], G.Wilkinson[36], M.Winter[10], M.Witek[19], O.Yushchenko[43], A.Zalewska[19], P.Zalewski[56], D.Zavrtanik[45], V.Zhuravlov[17], N.I.Zimin[17], A.Zintchenko[17], M.Zupan[12]

[1]Department of Physics and Astronomy, Iowa State University, Ames IA 50011-3160, USA

[2]IIHE, ULB-VUB, Pleinlaan 2, B-1050 Brussels, Belgium

[3]Physics Laboratory, University of Athens, Solonos Str. 104, GR-10680 Athens, Greece

[4]Department of Physics, University of Bergen, Allégaten 55, NO-5007 Bergen, Norway

[5]Dipartimento di Fisica, Università di Bologna and INFN, Via Irnerio 46, IT-40126 Bologna, Italy

[6]Centro Brasileiro de Pesquisas Físicas, rua Xavier Sigaud 150, BR-22290 Rio de Janeiro, Brazil

[7]Inst. de Física, Univ. Estadual do Rio de Janeiro, rua São Francisco Xavier 524, Rio de Janeiro, Brazil

[8]Collège de France, Lab. de Physique Corpusculaire, IN2P3-CNRS, FR-75231 Paris Cedex 05, France

[9]CERN, CH-1211 Geneva 23, Switzerland

[10]Institut de Recherches Subatomiques, IN2P3 - CNRS/ULP - BP20, FR-67037 Strasbourg Cedex, France

[11]Now at DESY-Zeuthen, Platanenallee 6, D-15735 Zeuthen, Germany

[12]Institute of Nuclear Physics, N.C.S.R. Demokritos, P.O. Box 60228, GR-15310 Athens, Greece

[13]FZU, Inst. of Phys. of the C.A.S. High Energy Physics Division, Na Slovance 2, CZ-180 40, Praha 8, Czech Republic

[14]Dipartimento di Fisica, Università di Genova and INFN, Via Dodecaneso 33, IT-16146 Genova, Italy

[15]Institut des Sciences Nucléaires, IN2P3-CNRS, Université de Grenoble 1, FR-38026 Grenoble Cedex, France

[16]Helsinki Institute of Physics and Department of Physical Sciences, P.O. Box 64, FIN-00014 University of Helsinki, Finland

[17]Joint Institute for Nuclear Research, Dubna, Head Post Office, P.O. Box 79, RU-101 000 Moscow, Russian Federation

[18]Institut für Experimentelle Kernphysik, Universität Karlsruhe, Postfach 6980, DE-76128 Karlsruhe, Germany

[19]Institute of Nuclear Physics PAN,Ul. Radzikowskiego 152, PL-31142 Krakow, Poland

[20]Faculty of Physics and Nuclear Techniques, University of Mining and Metallurgy, PL-30055 Krakow, Poland

[21]Université de Paris-Sud, Lab. de l'Accélérateur Linéaire, IN2P3-CNRS, Bât. 200, FR-91405 Orsay Cedex, France

[22]School of Physics and Chemistry, University of Lancaster, Lancaster LA1 4YB, UK

[23]LIP, IST, FCUL - Av. Elias Garcia, 14-1°, PT-1000 Lisboa Codex, Portugal

[24]Department of Physics, University of Liverpool, P.O. Box 147, Liverpool L69 3BX, UK

[25]Dept. of Physics and Astronomy, Kelvin Building, University of Glasgow, Glasgow G12 8QQ, UK

[26]LPNHE, IN2P3-CNRS, Univ. Paris VI et VII, Tour 33 (RdC), 4 place Jussieu, FR-75252 Paris Cedex 05, France

[27]Department of Physics, University of Lund, Sölvegatan 14, SE-223 63 Lund, Sweden

[28]Université Claude Bernard de Lyon, IPNL, IN2P3-CNRS, FR-69622 Villeurbanne Cedex, France

[29]Dipartimento di Fisica, Università di Milano and INFN-MILANO, Via Celoria 16, IT-20133 Milan, Italy

[30]Dipartimento di Fisica, Univ. di Milano-Bicocca and INFN-MILANO, Piazza della Scienza 3, IT-20126 Milan, Italy

[31]IPNP of MFF, Charles Univ., Areal MFF, V Holesovickach 2, CZ-180 00, Praha 8, Czech Republic

[32]NIKHEF, Postbus 41882, NL-1009 DB Amsterdam, The Netherlands

[33]National Technical University, Physics Department, Zografou Campus, GR-15773 Athens, Greece

[34]Physics Department, University of Oslo, Blindern, NO-0316 Oslo, Norway

[35]Dpto. Fisica, Univ. Oviedo, Avda. Calvo Sotelo s/n, ES-33007 Oviedo, Spain

[36]Department of Physics, University of Oxford, Keble Road, Oxford OX1 3RH, UK

[37]Dipartimento di Fisica, Università di Padova and INFN, Via Marzolo 8, IT-35131 Padua, Italy

[38]Rutherford Appleton Laboratory, Chilton, Didcot OX11 OQX, UK

[39]Dipartimento di Fisica, Università di Roma II and INFN, Tor Vergata, IT-00173 Rome, Italy

[40]Dipartimento di Fisica, Università di Roma III and INFN, Via della Vasca Navale 84, IT-00146 Rome, Italy

[41]DAPNIA/Service de Physique des Particules, CEA-Saclay, FR-91191 Gif-sur-Yvette Cedex, France

[42]Instituto de Fisica de Cantabria (CSIC-UC), Avda. los Castros s/n, ES-39006 Santander, Spain

[43]Inst. for High Energy Physics, Serpukov P.O. Box 35, Protvino, (Moscow Region), Russian Federation

[44]J. Stefan Institute, Jamova 39, SI-1000 Ljubljana, Slovenia

[45]Laboratory for Astroparticle Physics, University of Nova Gorica, Kostanjeviska 16a, SI-5000 Nova Gorica, Slovenia

[46]Department of Physics, University of Ljubljana, SI-1000 Ljubljana, Slovenia

[47]Fysikum, Stockholm University, Box 6730, SE-113 85 Stockholm, Sweden

[48]Dipartimento di Fisica Sperimentale, Università di Torino and INFN, Via P. Giuria 1, IT-10125 Turin, Italy

[49]INFN,Sezione di Torino and Dipartimento di Fisica Teorica, Università di Torino, Via Giuria 1, IT-10125 Turin, Italy

[50]Dipartimento di Fisica, Università di Trieste and INFN, Via A. Valerio 2, IT-34127 Trieste, Italy

[51]Istituto di Fisica, Università di Udine and INFN, IT-33100 Udine, Italy

[52]Univ. Federal do Rio de Janeiro, C.P. 68528 Cidade Univ., Ilha do Fundão BR-21945-970 Rio de Janeiro, Brazil

[53]Department of Radiation Sciences, University of Uppsala, P.O. Box 535, SE-751 21 Uppsala, Sweden

[54]IFIC, Valencia-CSIC, and D.F.A.M.N., U. de Valencia, Avda. Dr. Moliner 50, ES-46100 Burjassot (Valencia), Spain

[55]Institut für Hochenergiephysik, Österr. Akad. d. Wissensch., Nikolsdorfergasse 18, AT-1050 Vienna, Austria

[56]Inst. Nuclear Studies and University of Warsaw, Ul. Hoza 69, PL-00681 Warsaw, Poland

[57]Now at University of Warwick, Coventry CV4 7AL, UK

[58]Fachbereich Physik, University of Wuppertal, Postfach 100 127, DE-42097 Wuppertal, Germany

† deceased

1 Introduction

This paper presents the final interpretation of the Higgs boson search results from DELPHI in the framework of representative scenarios of the Minimal Supersymmetric Standard Model (MSSM). With respect to the previous MSSM interpretation published in Ref. [1], this analysis uses an enlarged set of experimental results, updated calculations of MSSM radiative corrections and covers more scenarios, including models with CP violation in the Higgs sector.

As compared with the Standard Model, the MSSM has an extended Higgs sector with two doublets of complex Higgs fields, leading to five physical Higgs bosons, of which three are neutral.
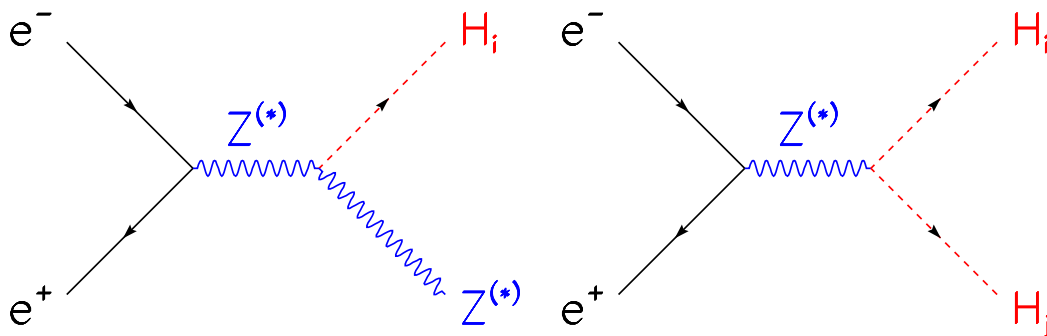
Figure 1: Main production processes of MSSM neutral Higgs bosons at LEP. Left: associated production of a Z and a Higgs boson, which must be one of the CP-even scalars (h or H) if CP is conserved or any Higgs boson (H_1, H_2, H_3) in the contrary case. At LEP1, the intermediate Z is on-shell and the final Z is off-shell, while it is the reverse at LEP2. Right: pair-production of neutral Higgs bosons. If CP is conserved, one of them must be CP-even (h or H) and the other one is the CP-odd pseudo-scalar A. If CP is not conserved, the pair can be any couple of different scalars among H_1, H_2 and H_3. The intermediate Z is on-shell at LEP1.

If CP is conserved, two of the three neutral Higgs bosons are CP-even. They are denoted h, for the lighter one, and H. The third one is a CP-odd pseudo-scalar, denoted A. In e^+e^- collisions, the dominant production mechanisms are the s-channel processes described in Fig. 1, that is the associated production of a Z and a CP-even Higgs boson and the pair production of either CP-even boson together with the CP-odd scalar. These processes are complemented by additional t-channel diagrams in the final states where a CP-even Higgs boson is produced with neutrinos or electrons, which proceed through W^+W^- and ZZ fusions, respectively. These diagrams and their interference with the H_iZ process have an impact on the production cross-section at masses around the H_iZ kinematic threshold. At LEP2 energies, the only significant effect is from W^+W^- fusion which doubles the neutrino H_iZ cross-section at the kinematic threshold. Finally, charged Higgs bosons, H^+ and H^-, are produced in pairs through a diagram similar to that in Fig. 1, right, via exchange of a Z boson or a photon.

Although CP is conserved at tree level in the MSSM, radiative corrections can introduce CP violation through stop and sbottom loops, leading to changes in the neutral Higgs boson sector [2]. If CP is not conserved, the three neutral Higgs bosons are no longer pure CP eigenstates but mixtures of CP-even and CP-odd components. They are

usually denoted H_1, H_2 and H_3, in increasing mass. The main production mechanisms are the same as in the CP conserving case, except that, *a priori*, any scalar can be produced in association with a Z boson or through W^+W^- and ZZ fusions, and any couple of different Higgs bosons can be pair-produced. The main phenomenological difference with respect to the CP-conserving case lies in the strength of the couplings of the Z boson to the Higgs scalars. In significant regions of the parameter space, CP violation turns off the otherwise dominant coupling between the Z boson and the lightest Higgs boson. In that case, if none of the other processes of Fig. 1 are possible (due e.g. to kinematics), the dominant Higgs boson production mechanism at LEP becomes the Yukawa process of Fig. 2. Of the two phases of LEP, only LEP1 has a significant sensitivity to this process. In the Standard Model, the corresponding cross-sections are negligible, e.g. a fraction of a pb for a few GeV/c^2 Higgs boson. In the MSSM, these can be enhanced by up to three orders of magnitude with respect to their Standard Model values, leading to detectable signals which become valuable in the case of CP violation.
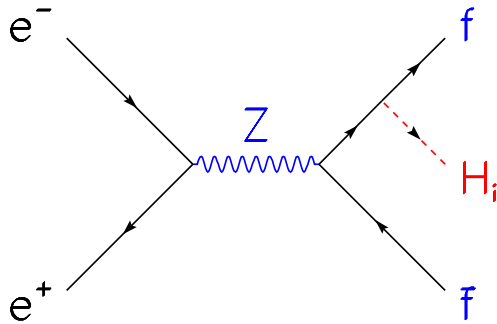
Figure 2: Additional production process of MSSM neutral Higgs bosons at LEP. The radiation of a Higgs boson off a Z boson decay fermion gives a detectable signal only at LEP1. This signal is exploited in the case of CP violation.

The decay properties of the Higgs bosons are moderately affected by CP violation, at least in the range of masses accessible at LEP, that is up to masses around $100 \, GeV/c^2$ [2]. In most of the MSSM parameter space of the scenarios studied hereafter, the three neutral Higgs bosons decay mainly into the pair of heaviest fermions kinematically permitted, even if CP is not conserved. Below the $\mu^+\mu^-$ threshold, a Higgs boson would decay into $\gamma\gamma$ or e^+e^- pairs with a significant lifetime. Above the $\mu^+\mu^-$ threshold, the lifetime is negligible and Higgs bosons decay at the primary vertex. Up to a mass of $3 \, GeV/c^2$ the main decays are into $\mu^+\mu^-$ pairs and also into hadronic channels with a large proportion of two-prong final states. Above $3 \, GeV/c^2$ the dominant decays are successively into $c\bar{c}$, $\tau^+\tau^-$ and finally $b\bar{b}$ pairs for Higgs boson masses above $12 \, GeV/c^2$. Besides these decays into fermions, there are also regions of the parameter space where one neutral Higgs boson can undergo cascade decays to a pair of Higgs bosons, as for example h $\rightarrow$ AA if CP is conserved or $H_2 \rightarrow H_1H_1$ in the contrary case. In some cases, especially if CP is not conserved, this mode dominates over the decays into SM particles. In the scenarios considered in this paper, charged Higgs bosons have a mass above $60 \, GeV/c^2$ and decay either into the pair of heaviest fermions allowed by kinematics, that is into cs or $\tau\nu$ pairs, or into a W^* and a light Higgs boson, e.g. into a W^*A pair if CP is conserved. Finally, these scenarios do not allow neutral or charged Higgs boson decays

into supersymmetric particles such as sfermions, charginos or invisible neutralinos. Note that searches for neutral Higgs bosons decaying into invisible products were performed at LEP, as reported in Ref. [3].

The different decay channels define the topologies that were searched for to cover the MSSM parameter region kinematically accessible at LEP energies. These topologies are described in Section 2. Section 3 summarizes the definition and techniques related to confidence levels used in the statistical interpretation of the searches. The eight CP-conserving MSSM benchmark scenarios studied in this analysis are presented in Section 4 and the results obtained in these scenarios when combining all searches are given in Section 5. Similarily, the CP-violating scenarios and the corresponding results are covered in Sections 6 and 7. The top quark mass has a significant impact on the properties of the Higgs bosons (e.g. mass spectrum of the neutral Higgs bosons, CP-violating effects). Results are thus derived for several values of this mass, namely: $m_{\text{top}} = 169.2, 174.3, 179.4$ and $183.0 \text{ GeV}/c^2$, which were defined after the measurement of the top quark mass at the Tevatron, run I [4]. Of the two values close to the present experimental measurement of $m_{\text{top}} = 170.9 \pm 1.1 \pm 1.5 \text{ GeV}/c^2$ [5], $174.3 \text{ GeV}/c^2$ gives the most conservative results and thus was chosen as a reference in most of the exclusion plots and to quote absolute mass and $\tan\beta$ limits. Readers interested in similar analyses at LEP are referred to Ref. [6,7].

2 Search channels

The different analyses performed to search for neutral and charged Higgs bosons in the whole LEP1 and LEP2 DELPHI data samples are summarized in Table 1 which lists the final states, mass ranges, integrated luminosities and the references for more details about the selections and their performance. Two channels, the $\tau^+\tau^- \text{b}\bar{\text{b}}$ signal at LEP1 and the $(\text{h} \rightarrow \text{AA} \rightarrow \text{c}\bar{\text{c}}\text{c}\bar{\text{c}})$ $(\text{Z} \rightarrow \text{q}\bar{\text{q}})$ signal at A masses below the $\text{b}\bar{\text{b}}$ threshold, were analysed for this paper, using selections already published. The efficiencies and the references for the selections can be found in the Appendices 1 and 2 of this paper. In the Table, the notations h and A which label the different analysis channels must be understood as generic notations for any pair of neutral Higgs bosons that could be produced in each of the production processes listed in the Table. As an example, the hZ analyses, originally designed to search for the CP-even h boson in CP-conserving scenarios, can be applied to search for the second CP-even Higgs boson, H, as well as for any of the three Higgs scalars in CP-violating scenarios. It must be noted that the kinematic properties of the signal processes are only slightly affected by CP-violation, since, when CP is not conserved, the production processes still proceed through the CP-even and CP-odd components of the neutral Higgs bosons, as explained in Ref. [7]. The same topological searches can thus be applied whether CP is conserved or not.

As compared with our previous publication [1], the following changes were introduced in the experimental results used. The MSSM interpretation in Ref. [1] relied only on searches performed at LEP2 at masses above 12 GeV/c^2 in m_{h} in the hZ process, with either direct or cascade decays, and above 40 GeV/c^2 in m_{h}, m_{A} in the hA channels, with only direct decays of the Higgs bosons. The corresponding channels have their $\sqrt{s}$ values in bold characters in Table 1. Scans of the MSSM parameter space were thus restricted to m_{A} above 12 GeV/c^2 and assumed the published LEP1 limits[1] to be valid. Including all LEP1 results, which have a sensitivity starting from vanishing h and A masses, and the additional LEP2 searches of Ref. [21], whose sensitivity in the hA mode

---

[1] $m_{\text{h}} > 44$ (46) GeV/c^2 when m_{h} is above (below) the AA threshold [14]

$\sqrt{s}$ (GeV)	final state	range (GeV/c^2)	$\mathcal{L}$ (pb^{-1})	disc. info.	ref.
	hZ with direct decays				
91	Z $\to$ e$^+$e$^-$, $\mu^+\mu^-$	< 0.21	2.5	no	[8]
91	(h $\to$ V^0) (Z $\to$ any)	< 0.21	2.5	no	[8]
91	(h $\to$ 2 prongs) (Z $\to$ q$\bar{\text{q}}$)	0.21 $-$ 2.	0.5	no	[9]
91	(h $\to$ jet) (Z $\to$ e$^+$e$^-$, $\mu^+\mu^-$)	1. $-$ 20.	0.5	no	[9]
91	(h $\to$ jet jet) (Z $\to$ l$^+$l$^-$, $\nu\bar{\nu}$)	> 12.	3.6	no	[10]
91	(h $\to$ jet jet) (Z $\to$ e$^+$e$^-$, $\mu^+\mu^-$, $\nu\bar{\nu}$)	> 35.	33.4	no	[11]
161,172	(h $\to$ b$\bar{\text{b}}$)(Z $\to$ any), (h $\to$ $\tau^+\tau^-$)(Z $\to$ q$\bar{\text{q}}$)	> 40.	19.9	1d	[17]
183	(h $\to$ b$\bar{\text{b}}$)(Z $\to$ any), (h $\to$ $\tau^+\tau^-$)(Z $\to$ q$\bar{\text{q}}$)	> 55.	52.0	1d	[18]
189	(h $\to$ b$\bar{\text{b}}$)(Z $\to$ any), (h $\to$ $\tau^+\tau^-$)(Z $\to$ q$\bar{\text{q}}$)	> 65.	158.0	2d	[19]
192-208	(h $\to$ b$\bar{\text{b}}$)(Z $\to$ any)	> 12.	452.4	2d	[20,1]
192-208	(h $\to$ $\tau^+\tau^-$)(Z $\to$ q$\bar{\text{q}}$)	> 50.	452.4	2d	[20,1]
189-208	(h $\to$ hadrons)(Z $\to$ any but $\tau^+\tau^-$)	> 4.	610.4	mix	[22]
	hA with direct decays				
91	4 prongs	> 0.4	5.3	no	[12]
91	$\tau^+\tau^-$ hadrons	> 8.	0.5	no	[13]
91	$\tau^+\tau^-$ jet jet	> 50	3.6	no	[10]
91	b$\bar{\text{b}}$b$\bar{\text{b}}$, b$\bar{\text{b}}$c$\bar{\text{c}}$	> 30.	33.4	no	[14]
91	$\tau^+\tau^-$b$\bar{\text{b}}$	> 16.	79.4	no	A.1
91	b$\bar{\text{b}}$b$\bar{\text{b}}$	> 24.	79.4	no	[21]
133	b$\bar{\text{b}}$b$\bar{\text{b}}$	> 80.	6.0	no	[16]
161,172	b$\bar{\text{b}}$b$\bar{\text{b}}$, $\tau^+\tau^-$b$\bar{\text{b}}$	> 80.	20.0	1d	[17]
183	b$\bar{\text{b}}$b$\bar{\text{b}}$, $\tau^+\tau^-$b$\bar{\text{b}}$	> 100.	54.0	1d	[18]
189	b$\bar{\text{b}}$b$\bar{\text{b}}$, $\tau^+\tau^-$b$\bar{\text{b}}$	> 130.	158.0	2d	[19]
192-208	$\tau^+\tau^-$b$\bar{\text{b}}$	> 120.	452.4	2d	[20,1]
192-208	b$\bar{\text{b}}$b$\bar{\text{b}}$	> 80.	452.4	2d	[20,1]
189-208	$\tau^+\tau^-\tau^+\tau^-$	> 8.	570.9	1d	[21]
189-208	b$\bar{\text{b}}$b$\bar{\text{b}}$	> 24.	610.2	no	[21]
189-208	hadrons	> 8.	610.4	mix	[22]
	hZ or hA with h $\to$ AA cascade				
91	Z $\to$ q$\bar{\text{q}}$	< 0.21	16.2	no	[15]
91	(AA $\to$ V^{0}V^0) (Z $\to$ any but $\tau^+\tau^-$)	< 0.21	9.7	no	[15]
91	(AA $\to$ $\gamma\gamma$) (Z $\to$ any or A $\to$ $\gamma\gamma$)	< 0.21	12.5	no	[15]
91	(AA $\to$ 4 prongs) (Z $\to$ any or A $\to$ 2 prongs)	> 0.21	12.9	no	[15]
91	(AA $\to$ hadrons) (Z $\to$ $\nu\bar{\nu}$ or A $\to$ hadrons)	> 0.21	15.1	no	[15]
91	(AA $\to$ $\tau^+\tau^-\tau^+\tau^-$) (Z $\to$ $\nu\bar{\nu}$ or A $\to$ $\tau^+\tau^-$)	> 3.5	15.1	no	[15]
161,172	(AA $\to$ any) (Z $\to$ q$\bar{\text{q}}$, $\nu\bar{\nu}$ or A $\to$ any)	> 20.	20.0	1d	[17]
183	(AA $\to$ b$\bar{\text{b}}$b$\bar{\text{b}}$) (Z $\to$ q$\bar{\text{q}}$)	> 12.	54.0	1d	[18]
192-208	(AA $\to$ b$\bar{\text{b}}$b$\bar{\text{b}}$, b$\bar{\text{b}}$c$\bar{\text{c}}$, c$\bar{\text{c}}$c$\bar{\text{c}}$) (Z $\to$ q$\bar{\text{q}}$)	> 12.	452.4	2d	[20,1]
192-208	(AA $\to$ c$\bar{\text{c}}$c$\bar{\text{c}}$) (Z $\to$ q$\bar{\text{q}}$)	> 4.	452.4	2d	A.2
189-208	(AA $\to$ b$\bar{\text{b}}$b$\bar{\text{b}}$) (Z $\to$ q$\bar{\text{q}}$ or A $\to$ b$\bar{\text{b}}$)	> 12.	610.2	no	[21]
	ffh or ffA Yukawa production				
91	bb(h $\to$ $\tau^+\tau^-$), bb(A $\to$ $\tau^+\tau^-$)	4. $-$ 50.	79.4	no	[21]
91	b$\bar{\text{b}}$(h $\to$ b$\bar{\text{b}}$), b$\bar{\text{b}}$(A $\to$ b$\bar{\text{b}}$)	11. $-$ 50.	79.4	no	[21]
91	$\tau^+\tau^-$(h $\to$ $\tau^+\tau^-$), $\tau^+\tau^-$(A $\to$ $\tau^+\tau^-$)	4. $-$ 50.	79.4	no	[21]
	H$^+$H$^-$				
189-208	c$\bar{\text{s}}\bar{\text{c}}s , cs\tau\nu_\tau$, W*A$\tau\nu_\tau$, W*AW*A	> 40.	610.4	2d	[23]
189-208	$\tau^+\nu_\tau\tau^-\bar{\nu}_\tau$	> 40.	570.8	1d	[23]

Table 1: List of signals expected from MSSM Higgs bosons that were searched for in the DELPHI data sample. Indicated for each signal are the centre-of-mass energy, final state, analysed mass range, integrated luminosity, level of discriminant information included in the confidence level estimates (none, one- or two-dimensional) and the reference where details of the analysis are published. Here h and A denote any neutral Higgs boson allowed to be produced in each of the indicated production processes. The mass range applies to m_{h} for hZ production, to $m_{\text{h}}+m_{\text{A}}$ for hA production, to m_{A} for h $\to$ AA processes, to the Higgs boson mass for either Yukawa process and to $m_{\text{H}^\pm}$ for H$^+$H$^-$ production. When no upper bound is given, the limit imposed by kinematics or vanishing branching fractions must be understood.

complements that of the two other sets of results, allows scans of the MSSM parameter space to be performed with no restriction on masses. Moreover, some of the analyses of Ref. [21] cover production processes which are negligible if CP is conserved but are enhanced by CP violation, such as Yukawa processes or the production of $\tau^+\tau^-\tau^+\tau^-$ final states. Adding the searches for neutral Higgs bosons decaying into hadrons of any flavour [22] is expected to provide sensitivity in scenarios where the Higgs boson decays into $b\bar{b}$ would vanish. As their mass coverage starts at low mass, these analyses also increase the experimental sensitivity to Higgs bosons below the $b\bar{b}$ threshold, a region otherwise covered only by analyses of subsets of the LEP1 data. Finally, the charged Higgs boson searches [23] help in a few CP-conserving scenarios in the low m_A region where the charged bosons are kinematically accessible at LEP2.

Moreover, our previous interpretation was dealing only with the production of the two lightest Higgs bosons, the h and A scalars in CP-conserving scenarios. In this analysis, the production of the third boson, if kinematically accessible, is also accounted for, which can lead to a significant gain in sensitivity in restricted areas of the parameter space. In CP-conserving scenarios, this leads to including the HZ and HA signals besides the usual hZ and hA processes, while in CP-violating models, the H_2Z and H_1H_3 signals are taken into account in addition to the dominant H_1Z and H_1H_2 channels (the two other processes, H_3Z and H_2H_3 being out of reach).

3 Tools for the statistical analysis

When scanning over the parameter space of a model, confidence levels are computed at each point to test the compatibility of data with the hypothesis of background only and with that of background plus signal as expected from the model. Throughout this section, the notations h, H and A must be understood as generic notations for the three neutral Higgs bosons of any type of MSSM scenario.

3.1 Confidence level definitions and calculations

The confidence levels are calculated using a modified frequentist technique based on the extended maximum likelihood ratio [24] which has also been adopted by the LEP Higgs working group. The basis of the calculation is the likelihood ratio test-statistic, $\mathcal{Q}$:

$$\ln \mathcal{Q} = -S + \sum_i \ln \frac{s_i + b_i}{b_i}$$

where S is the total signal expected and s_i and b_i are the signal and background densities for event i. These densities are constructed using either expected rates only or also additional discriminant information, which can be one- or two-dimensional. Table 1 presents the level of discriminant information for each channel: LEP1 results rely on rates only, while LEP2 results mix channels without or with discriminant information. As an example, in neutral Higgs boson channels with discriminant information, the first variable is the reconstructed Higgs boson mass in the hZ analyses and the sum of the reconstructed h and A masses in the hA analyses, while the second variable, if any, is channel-dependent, as specified in the references listed in the Table. Charged Higgs analyses use discriminant information in a similar way [23]. The searches for Higgs bosons decaying hadronically encompass analyses without or with 1d discriminant information together with analyses whose selections vary with the mass hypothesis [22].

The observed value of $\mathcal{Q}$ is compared with the expected Probability Density Functions (PDFs) for $\mathcal{Q}$, which are built using Monte Carlo sampling under the assumptions that background processes only or that both signal and background are present. The confidence levels CL_b and CL_{s+b} are their integrals from $-\infty$ to the observed value of $\mathcal{Q}$. Systematic uncertainties in the rates of signal or background events are taken into account in the calculation of the PDFs for $\mathcal{Q}$ by randomly varying the expected rates while generating the distribution [25], which has the effect of broadening the expected $\mathcal{Q}$ distribution and therefore making extreme events seem more probable.

CL_b is the probability of obtaining a result as background-like or more so than the one observed if the background hypothesis is correct. Similarly, the confidence level for the hypothesis that both signal and background are present, CL_{s+b}, is the probability, in this hypothesis, to obtain more background-like results than those observed. The quantity CL_s is defined as the ratio of these two probabilities, CL_{s+b}/CL_b. It is not a true confidence level, but a conservative pseudo-confidence level for the signal hypothesis. All exclusions discussed hereafter use CL_s and require it to be 5% for an exclusion confidence of 95%. As using CL_s instead of CL_{s+b} is conservative, the rate of fake exclusions is ensured to be below 5% when CL_s is equal to 5%.

3.2   Estimation of expected signal and background densities

The expected signal and background densities, which are required to check the consistency of the data with the background and signal processes have two components: the overall normalization which sets the expected rates and the Probability Density Functions (PDF) of the additional discriminant information, if any.

The expected background and signal rates were calculated from the number of simulated events passing the cuts. For the signal the efficiencies derived from simulations at given mass points had to be interpolated to estimate efficiencies at Higgs boson masses which were not simulated. In most cases this was done using one polynomial or if necessary two polynomials, one to describe the slow rise, and a second to handle the kinematic cut-off, which can be much more abrupt. For the cases where two signal masses must be allowed, a two-dimensional parameterization was used.

The shapes of the PDFs were derived using histograms which are taken from the simulated events. In the case of two-dimensional PDFs these distributions were smoothed using a two-dimensional kernel, which consists of a Gaussian distribution with a small component of a longer tail [26]. The global covariance of the distribution was used to determine the relative scale factors of the two axes. The width of the kernel varied from point to point, such that the statistical error on the estimated background processes was constant at 20%. Finally multiplicative correction factors (each a one-dimensional distribution for one of the two dimensions of the PDF) were derived such that when projected onto either axis the PDF has the same distribution as would have been observed if it had been projected onto the axis first and then smoothed. This makes better use of the simulation statistics if there are features which are essentially one-dimensional, such as mass peaks. The error parameter fixed to 20% was an important choice. It was set by dividing the background simulation into two subsamples, generating a PDF with one and using the other to test for over-training by calculating the CL_b obtained from simulation of background events. This should be 0.5 if the results are not to be biased, and a value of 20% for the error gave the closest approximation to 0.5 in all channels. Examples of smoothed two-dimensional PDFs are given in Fig. 3.

The signal simulations were made at fixed Higgs boson masses, but in order to test a continuous range of masses, interpolation software [27] was used to create signal PDFs at arbitrary masses. In the last year of operation, LEP energy was varied continuously while simulations were made at fixed beam energies. The same interpolation software was used to create signal and background PDFs at the correct centre-of-mass energies [1]. The interpolation was done by linearly interpolating the cumulative distributions taking as a parameter the signal mass or the centre-of-mass energy. The procedure has been tested over ranges up to 40 GeV/c^2 in mass while the actual shifts in the simulations were up to 0.3 GeV in $\sqrt{s}$, and 5 GeV/c^2 in mass for the hZ signals overall, but less than 0.5 GeV/c^2 for Higgs boson masses between 113.5 and 116.5 GeV/c^2. For the hA channels, the actual shifts were 5 GeV/c^2 in either mass for Higgs boson masses between 80 and 95 GeV/c^2 and up to 20 GeV/c^2 elsewhere. Comparisons of simulated and interpolated distributions for a given mass were made in all channels and showed good agreement.

3.3 The case of non-independent channels

When combining the results in all channels to derive confidence levels, only independent channels must be included, which requires some special treatment for a few non-independent cases.

a) different signals - one analysis with mass hypothesis-independent selections			
analysis	$\sqrt{s}$ (GeV)	signals added	ref.
ffh four-b	91	(bbh → bbbb), (bbA → bbbb), (hA → bbbb)	[21]
ffh b$\bar{\text{b}}\tau^+\tau^-$	91	(b$\bar{\text{b}}$h → b$\bar{\text{b}}\tau^+\tau^-$), (b$\bar{\text{b}}$A → b$\bar{\text{b}}\tau^+\tau^-$), (hA → b$\bar{\text{b}}\tau^+\tau^-$)	[21]
ffh four-τ	91	($\tau^+\tau^-$h → $\tau^+\tau^-\tau^+\tau^-$), ($\tau^+\tau^-$A → $\tau^+\tau^-\tau^+\tau^-$)	[21]
$\nu\bar{\nu}$q$\bar{\text{q}}$	161-172	(h → q$\bar{\text{q}}$) (Z → $\nu\bar{\nu}$), (h → AA) (Z → $\nu\bar{\nu}$)	[17]
$\tau^+\tau^-$q$\bar{\text{q}}$	189-208	(h → $\tau^+\tau^-$) (Z → q$\bar{\text{q}}$), (h → q$\bar{\text{q}}$) (Z → $\tau^+\tau^-$), (hA → $\tau^+\tau^-$q$\bar{\text{q}}$)	[19,20,1]
hZ four-jet	161-183	(h → q$\bar{\text{q}}$) (Z → q$\bar{\text{q}}$), (h → AA) (Z → q$\bar{\text{q}}$)	[17,18]
hZ four-jet	192-208	(h → q$\bar{\text{q}}$) (Z → q$\bar{\text{q}}$), (h → AA) (Z → q$\bar{\text{q}}$), (hA → b$\bar{\text{b}}$b$\bar{\text{b}}$)	[20,1]
hA four-jet	161-172	(hA → b$\bar{\text{b}}$b$\bar{\text{b}}$), (h → AA) A	[17]
hA four-jet	192-208	(hA → b$\bar{\text{b}}$b$\bar{\text{b}}$), (h → q$\bar{\text{q}}$) (Z → q$\bar{\text{q}}$)	[20,1]
four-b	189-208	(h → AA)A, (h → AA)Z, (hA → b$\bar{\text{b}}$b$\bar{\text{b}}$)	[21]
b) different analyses - one final state			
final state	$\sqrt{s}$ (GeV)	competing analyses	ref.
four-jet	91	bbbb, bbc$\bar{\text{c}}$	[14]
multi-jet	91	three and four-jet analyses	[21]
$\nu\bar{\nu}$q$\bar{\text{q}}$	192-208	low mass and high mass hZ analyses	[1]
	189-208	low mass and high mass flavour-blind analyses	[22]
	189-208	hZ and flavour-blind analyses	[19,20,1,22]
llq$\bar{\text{q}}$,l=e,μ	189-208	hZ and flavour-blind analyses	[19,20,1,22]
four-jet	192-208	low mass and high mass hZ analyses	[1]
	189-208	low mass and high mass hZ flavour-blind analyses	[22]
	189-208	three and four-jet hA flavour-blind analyses	[22]
	189-208	cscs and WAWA analyses	[23]
	189-208	hZ, hA, four-b, flavour-blind, c$\bar{\text{s}}\bar{\text{c}}$s and W*AW*A analyses	[19,20,1,21–23]
$\tau\nu$ jet jet	189-208	csν_τ and W*A$\tau\nu_\tau$ analyses	[23]

Table 2: a) list of signals from the two lightest Higgs bosons h and A treated by a single analysis: the signal expectations are combined (rates added, PDFs summed with weights according to the rates) prior to the confidence level calculations. b) list of different analyses of the same final state: only one analysis is selected at each point in the scans, based on the best expected performance for exclusion. In this Table, h and A denote any neutral Higgs boson allowed to be produced in the indicated production processes.

The first case is that of different signals covered by the same analysis. The treatment of this depended upon whether the analyses were themselves independent of the mass hypothesis for the Higgs bosons. The set of search channels (see Table 1) contains mostly analyses of this kind. In that case, all signals selected by one analysis were combined into one global channel prior to the confidence level computation. Expected rates were added together and PDFs were summed with weights given by the expected rates of the individual signals. As an illustration, Table 2-a gives the list of these signals and analyses on the example of the production of the lightest Higgs bosons, h and A, through the hZ and hA processes. When extending the combination to the third Higgs boson, H, the same procedure was followed, first for the various signals from that boson in the HZ and HA processes, and then to combine hZ and HZ signals or hA and HA signals. The PDF combination in such a case is illustrated in Fig. 3.

A different procedure was applied in the case of different signals covered by the same analysis whose selections do depend on the mass hypothesis, as most searches of Ref. [22] do. Different signals are covered by these analyses only when including signals from the third Higgs boson, H. In that case, in each analysis only one signal (from either h or H) was selected at each point in the scanned parameter space and at each centre-of-mass energy, on the basis of the smallest expected CL_s from experiments with no signal (that is, on the basis of the strongest average exclusion if no signal is present).

The second case of non-independent channels is that of a large overlap in the events selected by different analyses sensitive to the same final state. The list of such analyses and final states is detailed in Table 2-b. Again, for each final state, only that analysis with the strongest expected exclusion power was retained at each test point. This is not optimal but ensures that the channels which are then combined in the global confidence level computations are independent.

When the two cases just described (different signals covered by one analysis, different analyses sensitive to the same final state) were present simultaneously, the signal addition was performed before the final analysis selection. Then if that step involved more than two analyses, the final selection was made in successive iterations. To quote the four-jet final state as an example, at energies above 190 GeV, the total hZ and hA signals were first computed in each of the three four-jet analyses of Ref. [1] and in the four-b analysis of Ref. [21]. This summed three signals in the low and high mass hZ dedicated four-jet analyses ((h $\to$ q$\bar{q}$) (Z $\to$ q$\bar{q}$), (h $\to$ AA) (Z $\to$ q$\bar{q}$) and hA $\to$ b$\bar{b}$b$\bar{b}$), two signals in the hA dedicated four-jet analysis (hA $\to$ b$\bar{b}$b$\bar{b}$ and (h $\to$ q$\bar{q}$) (Z $\to$ q$\bar{q}$)) and three signals in the four-b analysis ((h $\to$ AA)A, (h $\to$ AA)(Z $\to$ q$\bar{q}$) and hA $\to$ b$\bar{b}$b$\bar{b}$). The signals due the third Higgs boson, H, were computed in the same way and added to those from the h boson. Then, a choice was made between the low and high mass hZ dedicated four-jet analyses. The result of this selection was compared with the hA dedicated four-jet analysis, and the best of these was confronted with the four-b analysis. A choice was made between the remaining analysis and the best between the various flavour-blind multi-jet analyses, that is the low mass and high mass hZ dedicated flavour-blind analyses, and the three and four-jet hA dedicated flavour-blind analyses [22]. As multi-jet flavour-blind analyses use mass-hypothesis dependent criteria, selecting the best one implied also a choice between the h and H signals for each of them. The analysis retained was finally compared with the result of the selection between the two charged Higgs multi-jet analyses, the cscs and WAWA dedicated analyses [23].
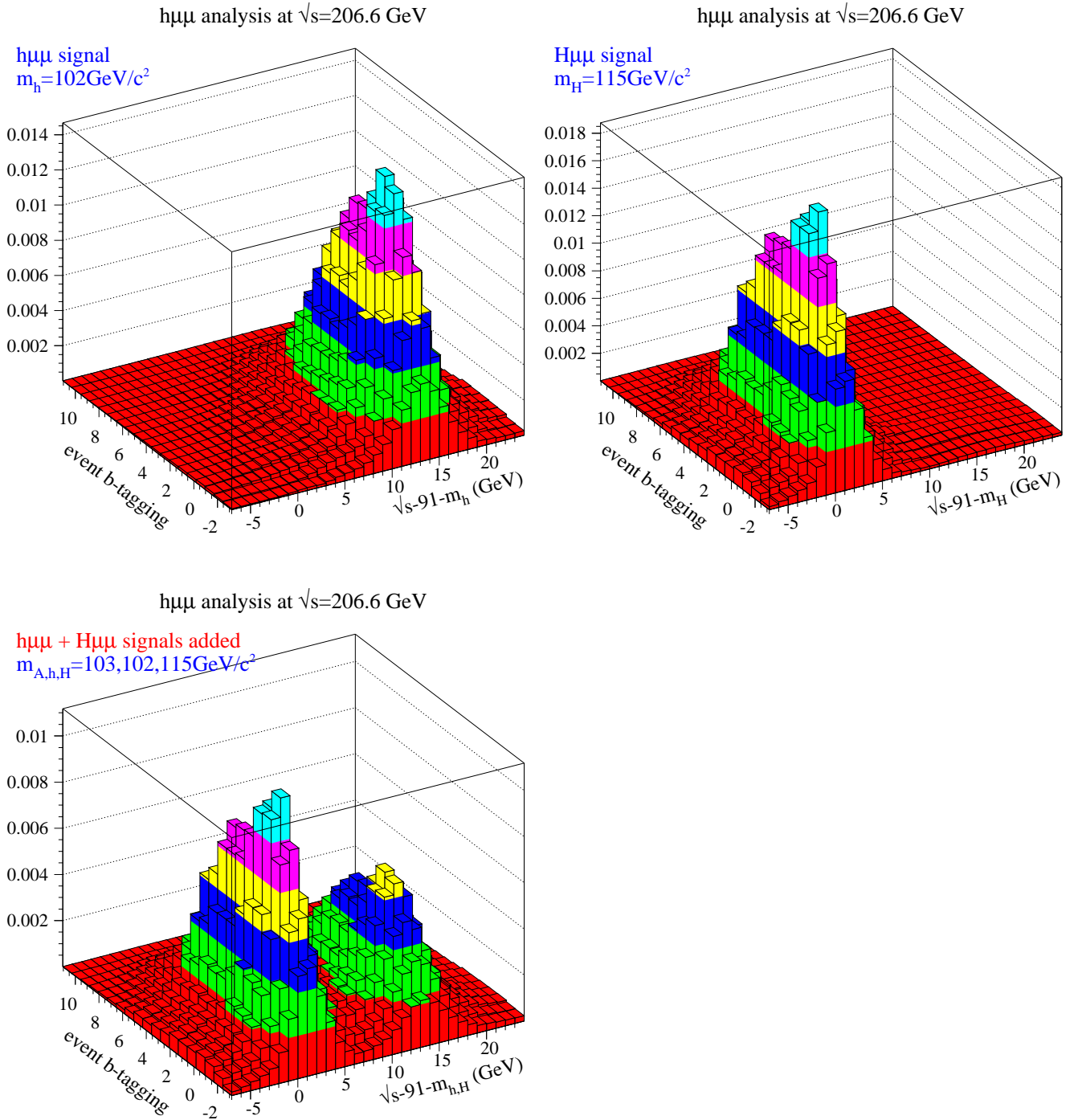
Figure 3: An example of two-dimensional PDFs from the analysis of the hZ $\rightarrow$ q$\bar{\text{q}}$ $\mu^+\mu^-$ channel at $\sqrt{s} = 206.6$ GeV [1]. The first discriminant variable is built from the reconstructed Higgs boson mass while the second is the event b-tagging variable. Top, left: PDF for a hZ signal with $m_\text{h} = 102$ GeV/c^2. Top, right: PDF for a HZ signal with $m_\text{H} = 115$ GeV/c^2. Bottom: PDF expected from the occurrence of both signals in a scenario where the expectations for the two signals are similar (cross-sections 32 and 42 fb, branching fractions into b$\bar{\text{b}}$ 92% and 91%, selection efficiencies 69% and 66% for hZ and HZ, respectively) leading to a double peak in the combined PDF.

4   The CP-conserving MSSM scenarios

In most of the parameter space of the CP-conserving MSSM scenarios, only hZ and hA productions are kinematically possible at LEP energies. These processes have complementary cross-sections since the hZZ and hAZ couplings are proportional to $\sin(\alpha - \beta)$ and $\cos(\alpha - \beta)$, respectively, where $\tan\beta$ is the ratio of the doublet vacuum expectation values and α is the Higgs doublet mixing angle which enters the definition of the two CP-even Higgs eigenstates as a mixture of the real, neutral components of the initial Higgs field doublets [2,28]. If kinematically allowed, hZ production dominates at low $\tan\beta$ or at large m_A, while in the rest of the parameter space, it is suppressed with respect to hA pair-production. The third neutral Higgs boson, H, in some scenarios and in limited regions of the parameter space, is light enough and can be produced with a large HZ or HA cross-section. As the HZZ coupling is proportional to $\cos(\alpha - \beta)$, and the HAZ one is proportional to $\sin(\alpha - \beta)$, HZ production, when allowed by kinematics, plays a role at large $\tan\beta$, and HA production at low $\tan\beta$. Similarily, charged Higgs bosons kinematically accessible at LEP2 energies are predicted in limited regions of the parameter space, typically when A is light, whatever $\tan\beta$. The minimal value of the mass of such charged Higgs bosons is 60 GeV/c^2 in the scenarios under study. The coverage of the region of the MSSM parameter space kinematically accessible at LEP is then assured primarily by the hZ and hA searches, with the help of the HZ, HA and to a lesser extent H$^+$H$^-$ channels.

At tree level, the production cross-sections and the Higgs branching fractions in the MSSM depend on two free parameters, usually chosen as $\tan\beta$ and one Higgs boson mass, or, alternatively, two Higgs boson masses, e.g. m_A and m_h. Radiative corrections introduce additional parameters related to supersymmetry breaking [2,28]. Hereafter, the usual assumption that some of them are equal at a given energy scale is made: hence, the SU(2) and U(1) gaugino mass parameters are assumed to be unified at the so-called GUT scale, while the sfermion mass parameters or the squark trilinear couplings are taken to be equal at the EW scale. Within these assumptions, the parameters beyond tree level are: the top quark mass, the Higgs mixing parameter, μ, which defines the Higgsino mass parameter at the EW scale, the common sfermion mass parameter at the EW scale, M_{susy}, the SU(2) gaugino mass parameter at the EW scale, M_2, the gluino mass, $m_{\tilde{g}}$, and the common squark trilinear coupling at the EW scale, A. The U(1) gaugino mass term at the EW scale, M_1, is related to M_2 through the GUT relation $M_1 = (5/3)\tan^2\theta_W M_2$. The radiative corrections affect the Higgs boson masses and couplings, with the largest contributions arising from loops involving the third generation quarks and squarks (top/stop and, at large values of $\tan\beta$, bottom/sbottom). As an example, the h boson mass, which is below that of the Z boson at tree level, increases by a few tens of GeV/c^2 in some regions of the MSSM parameter space due to radiative corrections.

4.1   The benchmark scenarios

In the following, eight benchmark scenarios are considered, as suggested in Ref. [29]. The values of their underlying parameters are quoted in Table 3. The first three scenarios are those usually studied at LEP. They have been proposed to test the sensitivity of LEP to Higgs bosons with either masses close to the kinematic limit or decays difficult to detect. Similarly, the five other scenarios are aimed at testing the sensitivity of the

scenario	M_{susy} (GeV/c^2)	M_2 (GeV/c^2)	$m_{\tilde{g}}$ (GeV/c^2)	μ (GeV/c^2)	X_t (GeV/c^2)
$m_{\mathrm{h}}^{\mathrm{max}}$	1000	200	800	-200	2 M_{susy}
no mixing	1000	200	800	-200	0
large μ	400	400	200	1000	-300
$m_{\mathrm{h}}^{\mathrm{max}}$, $\mu > 0$	1000	200	800	200	2 M_{susy}
$m_{\mathrm{h}}^{\mathrm{max}}$, $\mu > 0$, $X_t < 0$	1000	200	800	200	-2 M_{susy}
no mixing, $\mu > 0$, large M_{susy}	2000	200	800	200	0
gluophobic	350	300	500	300	-750
small α	800	500	500	2.5 M_{susy}	-1100

Table 3: Values of the underlying parameters for the eight representative MSSM scenarios scanned in this paper. Note that $X_t = A - \mu \cot \beta$. These scenarios have been studied for several values of the top quark mass, $m_{\mathrm{top}} = 169.2, 174.3, 179.4$ and 183.0 GeV/c^2.

Higgs boson searches at hadron colliders. It is thus interesting to establish the LEP constraints in such models too.

The first two scenarios, called the $m_{\mathrm{h}}^{\mathrm{max}}$ scenario and the no mixing scenario, differ only by the value of $X_t = A - \mu \cot \beta$, the parameter which controls the mixing in the stop sector (through the product $m_{\mathrm{top}}X_t$). This parameter has the largest impact on the mass of the h boson. The $m_{\mathrm{h}}^{\mathrm{max}}$ scenario leads to the maximum possible h mass as a function of $\tan \beta$. The no mixing scenario is its counterpart with vanishing mixing, leading to theoretical upper bounds on m_{h} which are at least 15 GeV/c^2 lower than in the $m_{\mathrm{h}}^{\mathrm{max}}$ scheme.

The third scenario is called the large μ scenario to account for a large, positive value of μ. As a consequence of the low value of M_{susy} and the moderate mixing in the stop sector, this scenario predicts at least one CP-even Higgs boson with a mass within kinematic reach at LEP2 in each point of the MSSM parameter space. However, there are regions for which detecting such a Higgs boson is difficult because of vanishing branching fractions into b-quarks. The values chosen for μ and X_t are indeed such that, in these regions, radiative corrections lead to suppressed couplings to b-quarks for one or the other CP-even Higgs boson. The dominant decays in these regions being still into hadrons, the main analysis channels suffer from large backgrounds. This scenario was designed to test the sensitivity of LEP through analyses that could not benefit from the b-tagging capabilities of the experiments.

Among the five other benchmark scenarios, three are variants of the $m_{\mathrm{h}}^{\mathrm{max}}$ and no mixing scenarios. The sign of μ and that of the mixing parameter have been reversed in the two scenarios derived from the LEP $m_{\mathrm{h}}^{\mathrm{max}}$ scenario. The changes in the Higgs boson mass spectrum and properties are small. The sign of μ has been reversed and the value of M_{susy} has been doubled in the scenario derived from the no mixing scenario of LEP. The higher M_{susy} scale leads to a few GeV/c^2 increase of the theoretical upper bound on m_{h}. The last two scenarios have been proposed to test potentially difficult cases for the searches at hadron colliders. Hence, the gluophobic scenario presents regions where the main production channel at the LHC, gluon fusion, is suppressed due to cancellations between the top quark and stop quark loops in the production process. Finally, in the small α scenario, important decay channels at the Tevatron and at the LHC, h $\to$ b$\bar{\mathrm{b}}$ and h $\to \tau^+\tau^-$, are suppressed at large $\tan \beta$ and moderate m_{A}. In these regions, the radiatively corrected mixing angle α is low, resulting in suppressed couplings

scenario	m_{top} (GeV/c^2)			
	169.2	174.3	179.4	183.0
$m_{\text{h}}^{\text{max}}$	128.2	132.9	138.6	142.7
no mixing	**112.8**	**115.5**	118.2	120.3
large μ	**106.1**	**108.0**	**110.1**	**111.6**
$m_{\text{h}}^{\text{max}}$, $\mu > 0$	128.4	134.1	140.1	144.3
$m_{\text{h}}^{\text{max}}$, $\mu > 0$, $X_t < 0$	124.5	128.8	134.3	138.2
no mixing, $\mu > 0$, large M_{susy}	**117.0**	120.2	123.7	126.3
gluophobic	**115.7**	118.8	122.0	124.4
small α	118.5	122.2	126.2	129.1

Table 4: Maximal value of m_{h} (in GeV/c^2) in the eight benchmark MSSM scenarios studied in this paper, as a function of m_{top}. Radiative corrections include all dominant second-order loop terms [30]. The maximum value of m_{h} corresponds approximately to the minimum value of the mass of the third Higgs boson, H. Bold values indicate scenarios where this boson is kinematically accessible at LEP.

of the ligthest CP-even Higgs boson to down-type fermions since these couplings are proportional to $-\sin\alpha/\cos\beta$.

In all scenarios, the radiative corrections have been computed in the Feynman-diagrammatic approach with all dominant two-loop order terms included, using version 2.0 of the FEYNHIGGS code [30]. As a first illustration of the different scenarios, Table 4 gives the maximum value of m_{h} allowed by theory in each of them, for the four values of m_{top} studied in this paper. At a given m_{top} value, the three $m_{\text{h}}^{\text{max}}$ scenarios give the highest upper bounds on m_{h}, the positive μ scenario leading to the maximal value. The large μ scenario presents the lowest upper bound, followed in increasing order by the no mixing scenario, the gluophobic one, the no mixing scenario with positive μ and the small α scheme. The maximum value of m_{h} increases significantly with m_{top}. The effect is most important in the three $m_{\text{h}}^{\text{max}}$ scenarios, and is much smaller in the others, especially in the large μ scheme. It must be noted that the maximum value of m_{h} corresponds approximately to the minimum value of m_{H} in regions of large HZZ couplings (see Fig.4). Thus, there are a few scenarios where the H signal is expected to contribute to the experimental sensitivity. These are indicated in bold characters in Table 4.

To illustrate further the Higgs boson phenomenology at LEP, a few properties are compared in Fig. 4 in the case of the no mixing and $m_{\text{h}}^{\text{max}}$ scenarios for a top quark mass of 174.3 GeV/c^2. The figures showing masses and cross-sections underline the importance of the signal from the heavy scalar, H, which can be kinematically accessible at LEP2 energies with a large HZ production cross-section at large $\tan\beta$ and moderate m_{A}, up to about 100 GeV/c^2. The width curves demonstrate that, at large $\tan\beta$, neutral Higgs bosons can have a width exceeding the experimental resolution which is of the order of 1 to 3 GeV/c^2 depending on the search channel. At moderate m_{A}, this affects the h and A bosons and thus the hA production mode, but not the HZ one. At large m_{A}, width effects become negligible for the h boson so that the hZ production mode, which is the only possible dominant mode in that region, is not affected. The figures showing branching fractions compare the no mixing and $m_{\text{h}}^{\text{max}}$ scenarios at low $\tan\beta$. In both scenarios, the h branching fraction into b$\bar{\text{b}}$ decreases to the profit of that into AA at very low $\tan\beta$, but the residual b$\bar{\text{b}}$ branching ratio is significantly higher in the $m_{\text{h}}^{\text{max}}$ scenario.
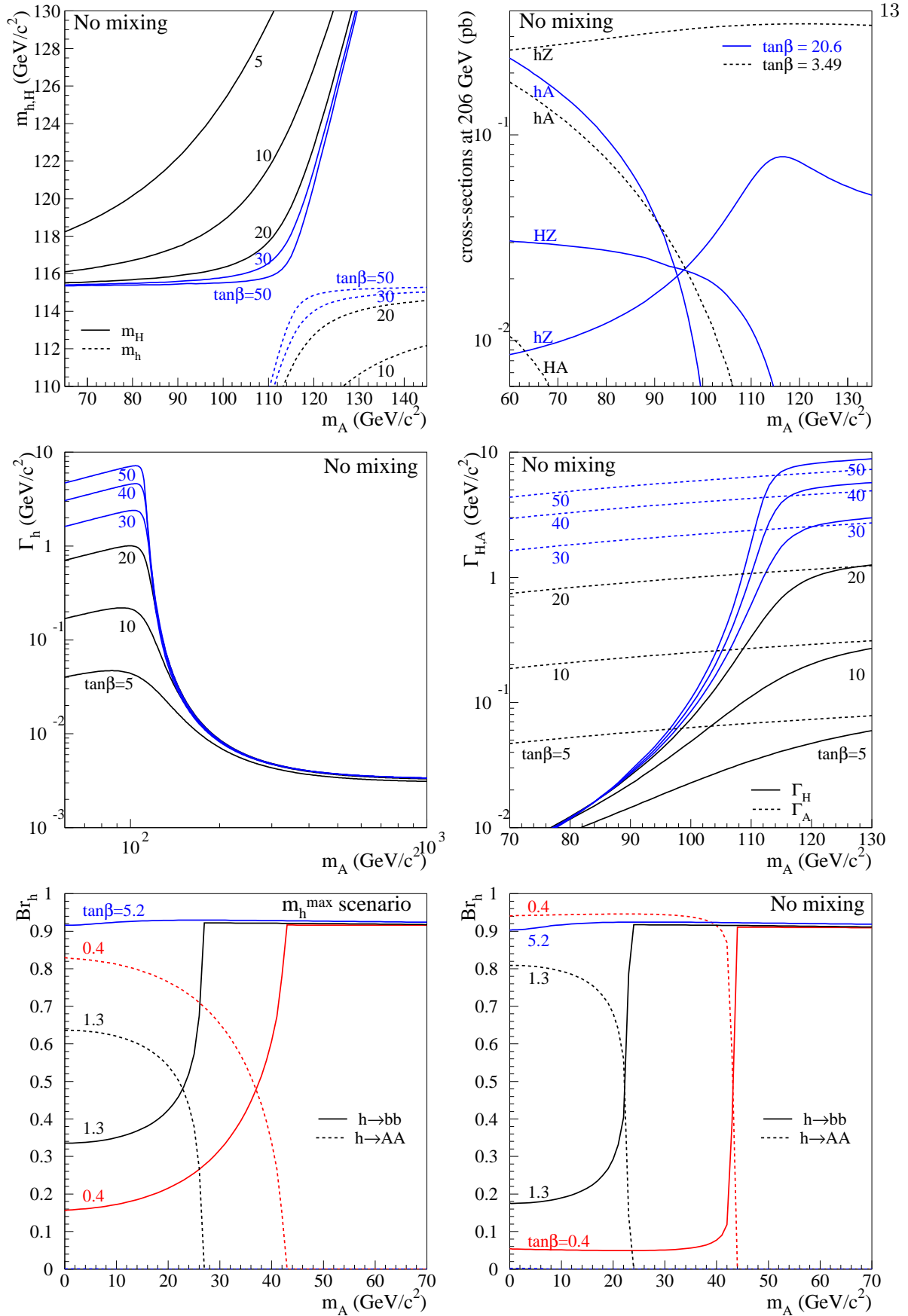
Figure 4: Properties of the three neutral Higgs bosons of the CP-conserving MSSM in the no mixing and m_h^{max} scenarios with $m_{top} = 174.3$ GeV/c^2. Top: H and h masses and H, h and A production cross-sections at $\sqrt{s} = 206$ GeV, at various $\tan\beta$ values. Middle: h, H and A widths as a function of m_A and $\tan\beta$. Bottom: h branching fractions as a function of m_A at low to moderate values of $\tan\beta$. Decays into $b\bar{b}$ (solid lines) and AA (dashed lines) are compared. All dominant two-loop order radiative corrections are included [30].

Finally, it should be noted that our previous MSSM interpretation of Ref. [1] relied on partial two-loop order radiative corrections [31]. In the present paper, these have been updated to include all dominant two-loop order corrections [30]. This leads to significant changes in the Higgs boson masses and properties. The main effect is an increase of the maximum (resp. minimum) allowed value of the h (resp. H) boson mass at fixed $\tan\beta$. As a consequence, the experimental sensitivity in $\tan\beta$ and that in m_{H} are expected to decrease. A review of the changes induced by the more complete corrections on the experimental sensitivity of DELPHI is given in Ref. [32,33] in the framework of the three LEP scenarios, keeping identical experimental inputs.

4.2 Scan procedure

In each scenario, a scan was performed over the MSSM parameters $\tan\beta$ and m_{A}. The range in m_{A} spans from 0.02 GeV/c^2 up to 1 TeV/c^2. Values of m_{A} leading to unphysical negative mass squared values were removed from the scans. Such points are rather rare, except in the large μ, gluophobic and small α scenarios (see section 5). The range in $\tan\beta$ extends from the minimal value allowed in each scenario[2] up to 50, a value chosen in the vicinity of the ratio of the top- and b-quark masses, above which the Higgs-bottom Yukawa coupling is expected to become unreliable (see e.g. [2]). The scan steps were 1 GeV/c^2 in m_{A} and 0.1 in $\tan\beta$ in the regions where m_{h} varies rapidly with these parameters. At low m_{A}, where the decay modes change rapidly with the Higgs boson mass, values tested were 0.02, 0.1, 0.25, 0.5, 1.5 and 3 GeV/c^2.

At each point of the parameter space, the neutral and charged Higgs cross-sections and their branching fractions were taken from databases provided by the LEP Higgs working group [7], on the basis of the theoretical calculations in Ref. [30], completed by that in Ref. [34] for the charged Higgs boson branching fractions. The signals from the third Higgs boson, H, were included in the channel combination at each point where m_{H} was found to be below 120 GeV/c^2, the ultimate sensitivity of LEP. The signal expectations in each channel were then derived from the theoretical cross-sections and branching fractions, the experimental luminosity and the efficiencies. If necessary, a correction was applied to account for different branching fractions of the Higgs bosons between the test point and the simulation (e.g. for the hZ and HZ processes, the simulation was done in the SM framework).

As stated in the previous section, neutral Higgs bosons can have non-negligible widths at large $\tan\beta$ when m_{A} is above a few tens of GeV/c^2. In this region, the experimental sensitivity is dominated by the LEP2 hA analyses dedicated to standard MSSM final states. To account for width effects in these channels, efficiencies derived from simulations with h and A widths below 1 GeV/c^2 (see e.g. Ref. [1]) were applied for $\tan\beta <$ 30 only. Above that value, efficiencies were linearly interpolated in $\tan\beta$ between the efficiencies from these simulations and those from simulations at $\tan\beta = 50$ where the Higgs boson widths exceed the experimental resolution. As the Higgs boson widths grow approximately linearly with $\tan\beta$ above 30, a linear interpolation is valid. The same holds for the discriminant information, for which the same interpolation software was used as discussed in section 3.2 for the PDF interpolation in mass or centre-of-mass energy. The effect of the Higgs boson widths on the PDFs of the hA signals and the interpolation in $\tan\beta$ of these PDFs are illustrated in Fig. 5. Note that the hZ and HZ channels at large $\tan\beta$ are not affected by such an effect since in most of the regions where they possibly contribute, their widths are below the experimental resolution, as shown in Fig. 4.

---

[2]The minimal value of $\tan\beta$ is around 0.7 in the large μ scenario and in the no mixing scenario with positive μ and 0.4 in all other schemes. Lower $\tan\beta$ values give rise to unphysical negative mass squared values in the Higgs sector.
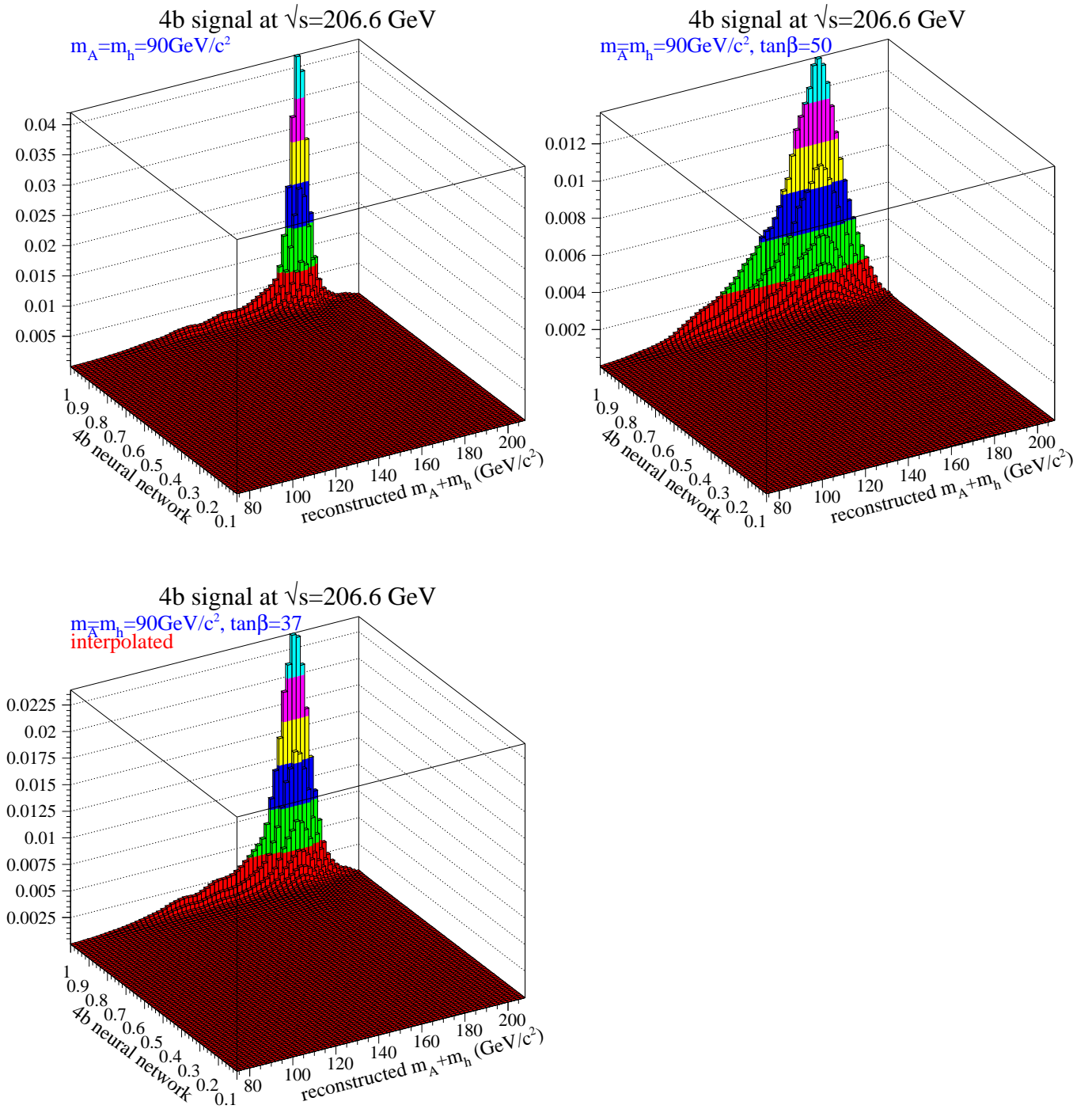
Figure 5: Two-dimensional PDFs used in the analysis of the hA → b$\bar{\text{b}}$b$\bar{\text{b}}$ channel at $\sqrt{s}$ = 206.6 GeV [1]. The first discriminant variable is the sum of the reconstructed Higgs boson masses while the second is a neural network output. Top, left: PDF for a hA signal with $m_A = m_h = 90$ GeV/c^2 and h and A widths below 1 GeV/c^2. Top, right: PDF for a hA signal with $m_A = m_h = 90$ GeV/c^2 and $\tan\beta = 50$. The Higgs boson widths in that case are 5 and 9 GeV/c^2 for A and h, respectively. Bottom: PDF linearly interpolated in $\tan\beta$ at a value of 37.

5 Results in CP-conserving MSSM scenarios

The regions of the MSSM parameter space excluded at 95% CL or more by combining the searches of Table 1 are hereafter discussed in turn for each scenario. The exclusion is dominated by the searches for neutral Higgs bosons in standard MSSM final states. The searches for neutral Higgs bosons decaying into hadrons of any flavour and the charged Higgs boson searches complete the exclusion in restricted regions of the parameter space. In addition, the limit on the Z partial width that would be due to new physics [35], $\Gamma^{\mathrm{new}} < 6.6$ MeV/c^2 is used as an external constraint on the hA process at LEP1. A detailed account of the impact of these auxiliary constraints can be found in Ref. [33,36].

5.1 The $m_{\mathrm{h}}^{\mathrm{max}}$ scenario

The excluded regions in the $m_{\mathrm{h}}^{\mathrm{max}}$ scenario are presented in the $(m_{\mathrm{h}}, \tan\beta)$, $(m_{\mathrm{A}}, \tan\beta)$ and $(m_{\mathrm{h}}, m_{\mathrm{A}})$ planes in Fig. 6 for a top mass value of 174.3 GeV/c^2. Basically, the exclusion is made by the results in the hZ (hA) channels in the low (large) $\tan\beta$ region while they both contribute at intermediate values. The searches for the heavy scalar, H, brings no additional sensitivity since H is not kinematically accessible in this scenario (see Table 4). The above results establish the following 95% CL lower limits on m_{h} and m_{A} for $m_{\mathrm{top}} = 174.3$ GeV/c^2:

$$m_{\mathrm{h}} > 89.7 \text{ GeV}/c^2 \qquad m_{\mathrm{A}} > 90.4 \text{ GeV}/c^2$$

for any value of $\tan\beta$ between 0.4 and 50. The expected median limits are 90.6 GeV/c^2 for m_{h} and 90.8 GeV/c^2 for m_{A}. The observed limit in m_{A} (m_{h}) is reached at $\tan\beta$ around 20 (10), in a region where both the hZ and hA processes contribute. For $m_{\mathrm{top}} = 174.3$ GeV/c^2 the range in $\tan\beta$ between 0.7 and 1.9 (expected [0.7-1.9]) is excluded for any value of m_{A} between 0.02 and 1000 GeV/c^2. These limits and exclusions, as well as those for all the CP-conserving scenarios, are summarized in Table 5.

The m_{top} dependence of the above limits was also studied, as reported in Table 5. The mass limits remain unchanged when varying m_{top}, for m_{h} is insensitive to m_{top} in the region of large $\tan\beta$ and intermediate m_{A} where the limits are set. On the other hand, the excluded range in $\tan\beta$ is governed by the maximal value of m_{h}, which is reached at large m_{A} where m_{h} is very sensitive to m_{top}, as illustrated in the top left-hand plot in Fig. 6: hence the variation of the limits in $\tan\beta$ as reported in Table 5 and Fig. 14. An exclusion in $\tan\beta$ exists for a top mass up to 179.4 GeV/c^2 which is about three standard deviations higher than the current average m_{top} measurement. The exclusion would vanish for a top mass as high as 183.0 GeV/c^2.

5.2 The $m_{\mathrm{h}}^{\mathrm{max}}$ scenario but with μ positive and either sign for X_t

The excluded regions for a top mass value of 174.3 GeV/c^2 are presented in Fig. 7 for the $m_{\mathrm{h}}^{\mathrm{max}}$ scenario with positive μ, keeping X_t positive as in the original $m_{\mathrm{h}}^{\mathrm{max}}$ scenario, and in Fig. 8 for the $m_{\mathrm{h}}^{\mathrm{max}}$ scenario with positive μ and negative X_t. The results are quite similar to those in the original $m_{\mathrm{h}}^{\mathrm{max}}$ scenario. Mass limits are within 200 MeV/c^2 of those in the previous section and do not vary significantly with m_{top}, as reported in Table 5.

To compare observed and median limits, the 95% CL lower limits on m_{h} and m_{A} in the $m_{\mathrm{h}}^{\mathrm{max}}$ scenario with positive μ for $m_{\mathrm{top}} = 174.3$ GeV/c^2 are:
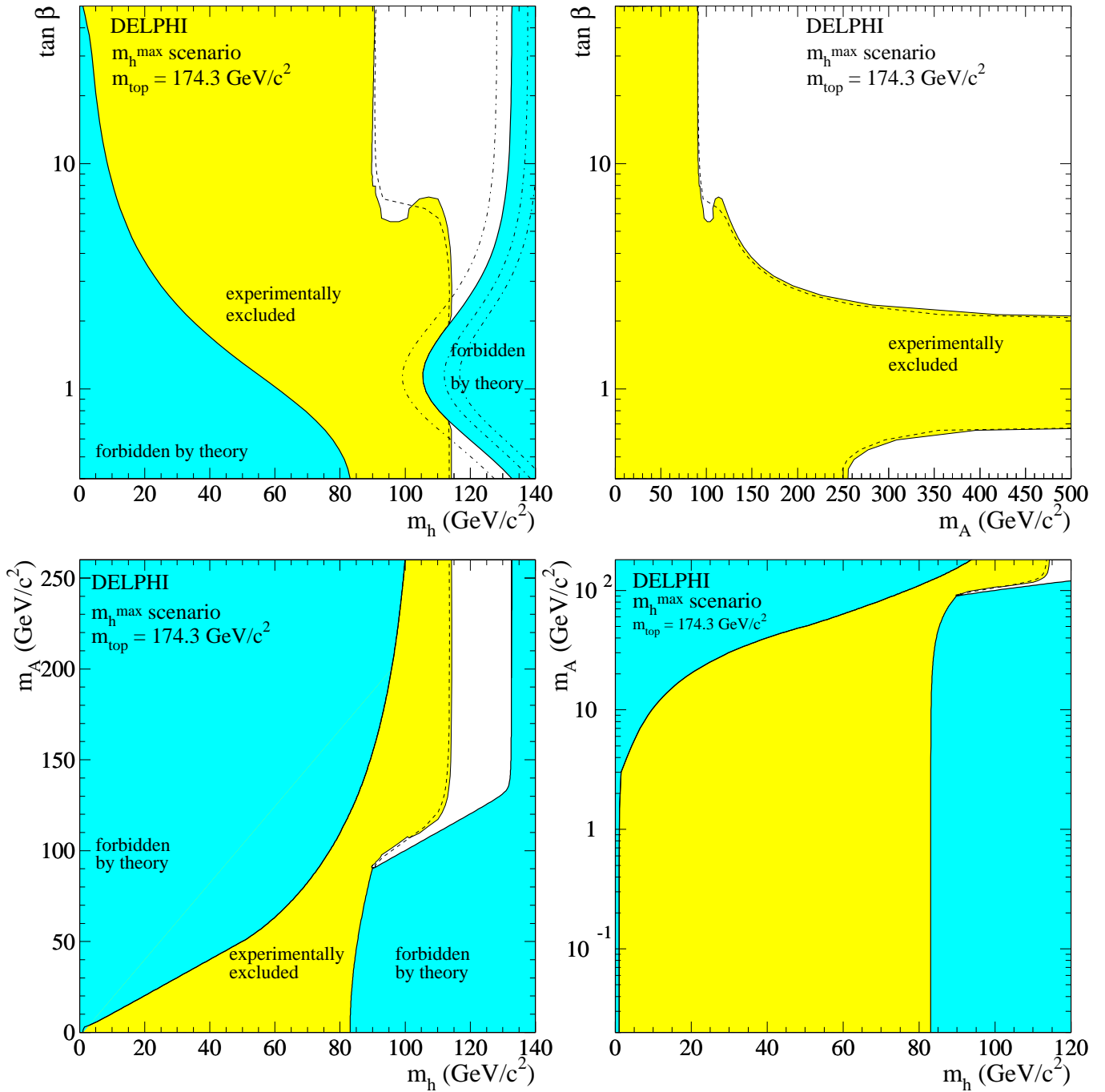
Figure 6: MSSM m_h^{max} scenario for a top mass of 174.3 GeV/c^2: regions excluded at 95% CL by combining the results of the Higgs boson searches in the whole DELPHI data sample (light-grey). The dashed curves show the median expected limits. The medium-grey areas are the regions not allowed by theory. The dash-dotted lines in the top left-hand plot are the theoretical upper bounds for a top mass of 169.2, 179.4 and 183.0 GeV/c^2 (from left to right).

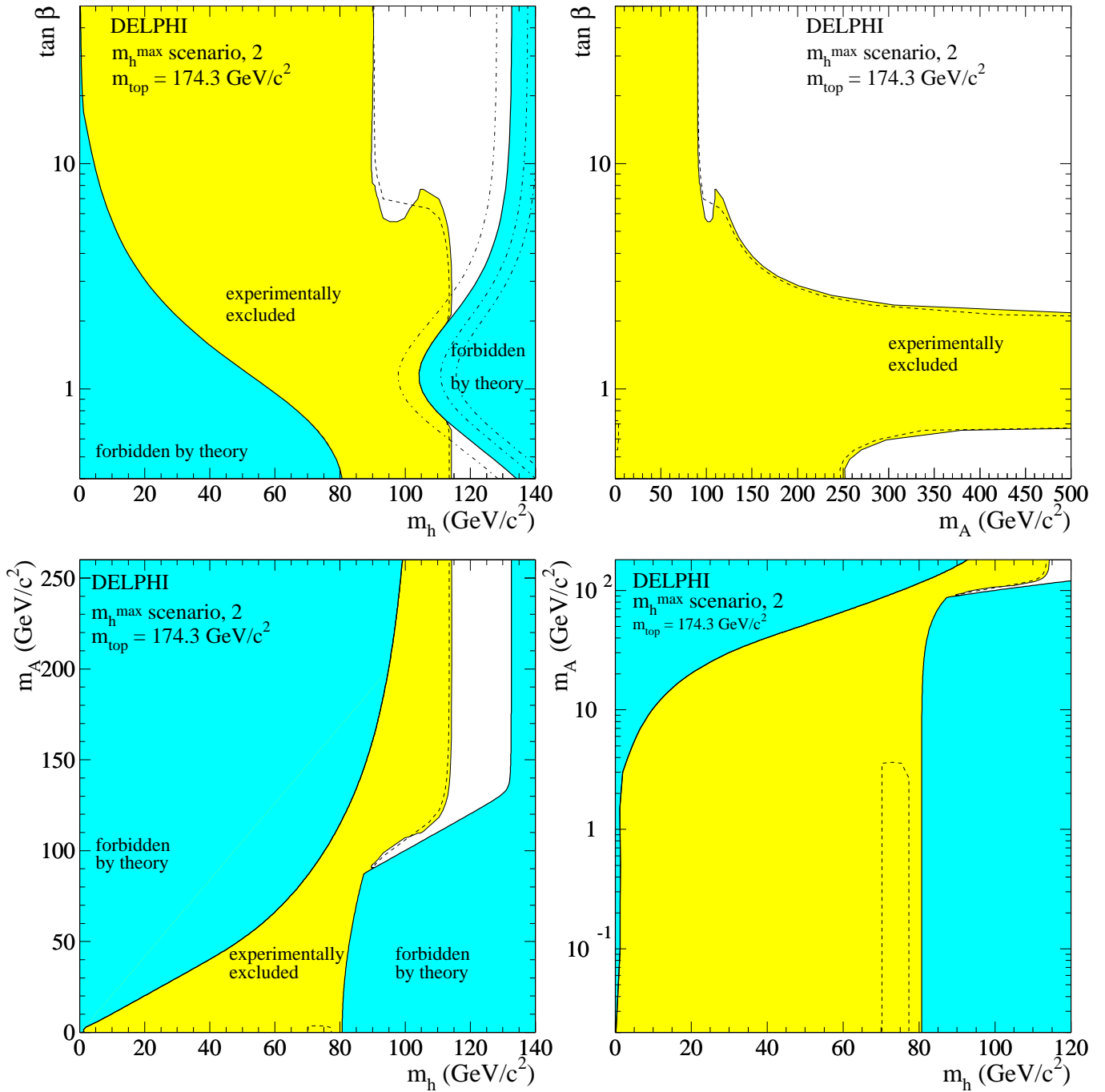Figure 7: MSSM $m_\mathrm{h}^\mathrm{max}$ scenario with positive μ for a top mass of 174.3 GeV/c^2: regions excluded at 95% CL by combining the results of the Higgs boson searches in the whole DELPHI data sample (light-grey). The dashed curves show the median expected limits. The medium-grey areas are the regions not allowed by theory. The dash-dotted lines in the top left-hand plot are the theoretical upper bounds for a top mass of 169.2, 179.4 and 183.0 GeV/c^2 (from left to right).
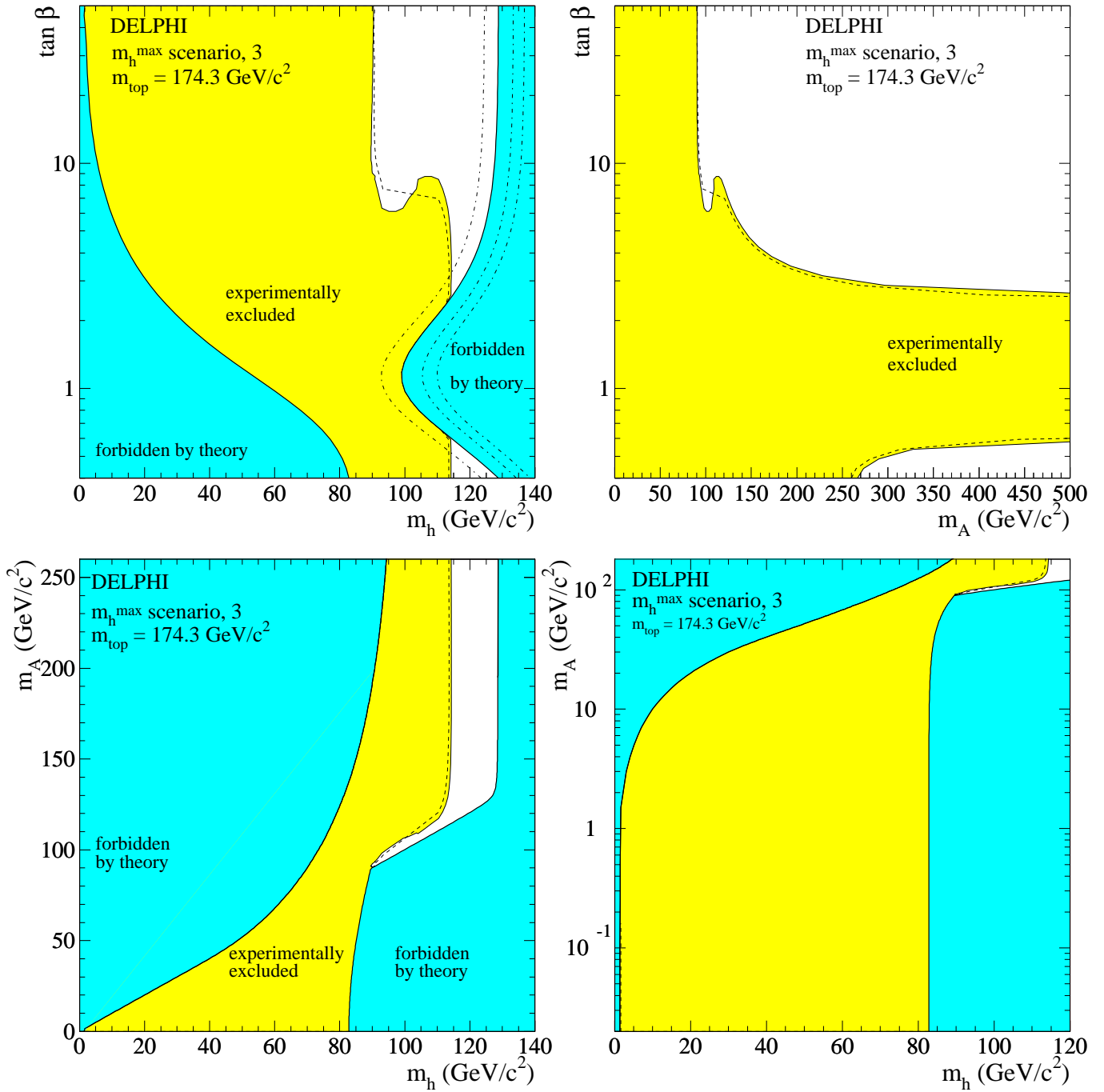
Figure 8: MSSM m_h^{max} scenario with positive μ and negative X_t for a top mass of 174.3 GeV/c^2: regions excluded at 95% CL by combining the results of the Higgs boson searches in the whole DELPHI data sample (light-grey). The dashed curves show the median expected limits. The medium-grey areas are the regions not allowed by theory. The dash-dotted lines in the top left-hand plot are the theoretical upper bounds for a top mass of 169.2, 179.4 and 183.0 GeV/c^2 (from left to right).

$$m_{\mathrm{h}} > 89.6 \text{ GeV}/c^2 \qquad m_{\mathrm{A}} > 90.3 \text{ GeV}/c^2$$

for any value of $\tan\beta$ between 0.4 and 50. The expected median limits are 90.3 GeV/c^2 for m_{h} and 90.4 GeV/c^2 for m_{A}. The 95% CL lower limits on m_{h} and m_{A} in the $m_{\mathrm{h}}^{\mathrm{max}}$ scenario with positive μ and negative X_t for $m_{\mathrm{top}} = 174.3$ GeV/c^2 are:

$$m_{\mathrm{h}} > 89.6 \text{ GeV}/c^2 \qquad m_{\mathrm{A}} > 90.4 \text{ GeV}/c^2$$

for any value of $\tan\beta$ between 0.4 and 50. The expected median limits are 90.4 GeV/c^2 for m_{h} and 90.6 GeV/c^2 for m_{A}.

The excluded ranges in $\tan\beta$ are different in the three $m_{\mathrm{h}}^{\mathrm{max}}$ scenarios, since they have different theoretical upper bounds on m_{h}. For $m_{\mathrm{top}} = 174.3$ GeV/c^2 the excluded range in the $m_{\mathrm{h}}^{\mathrm{max}}$ scenario with positive μ lies between 0.7 and 2.0 (expected [0.8-2.0]), while in the $m_{\mathrm{h}}^{\mathrm{max}}$ scenario with positive μ and negative X_t it spans from 0.6 to 2.5 (expected [0.6-2.4]). These limits are valid for any value of m_{A} between 0.02 and 1000 GeV/c^2. Note that despite the higher maximal value of m_{h} in the $m_{\mathrm{h}}^{\mathrm{max}}$ scenario with positive μ, the most conservative limits in $\tan\beta$ are still derived in the original $m_{\mathrm{h}}^{\mathrm{max}}$ scenario (see Section 5.1), reflecting the differences in the theoretical upper bounds at $\tan\beta$ around 1 (see top left-hand plots in Fig. 6, 7 and 8). The m_{top} dependence of the above limits is presented in Table 5 and Fig. 14. For a top mass as high as 183 GeV/c^2, there would be no longer any exclusion in $\tan\beta$ in the $m_{\mathrm{h}}^{\mathrm{max}}$ scenario with positive μ, while there is still one in the scenario with positive μ and negative X_t due to the lower maximal value of m_{h} in that scenario.

5.3 The no mixing scenario

The excluded regions in the no mixing scenario are presented in Fig. 9 for a top mass value of 174.3 GeV/c^2. In this scenario, if the top is not too heavy, the heavy scalar, H, is kinematically accessible at large $\tan\beta$ and moderate m_{A}, the region where the mass limits in m_{A} and m_{h} are set. Thus, allowing for its production increases the sensitivity of the searches.

The zoom at low m_{A} in the (m_{h}, m_{A}) projection shows that the direct searches leave three unexcluded regions below 12 GeV/c^2 in m_{A}. The thin strip along the theoretical lower bound on m_{h} at very low m_{A} (hardly visible in the figure) is excluded by the limit on the Z partial width that would be due to new physics [35], $\Gamma^{\mathrm{new}} < 6.6$ MeV/c^2, which, when applied to the hA process, translates into an excluded region that encompasses that area. This is not the case for the two other unexcluded regions. These have $\tan\beta$ below 1.0 and m_{h} between 59 and 82 GeV/c^2. In that region, m_{A} is below the kinematic threshold $m_{\mathrm{h}} = 2m_{\mathrm{A}}$, the decay h $\to$ AA opens and supplants the h $\to$ b$\bar{\mathrm{b}}$ mode, as can be seen in Fig. 4. Our LEP2 h $\to$ AA searches, covering A masses above the c$\bar{\mathrm{c}}$ threshold (see Table 1), have no sensitivity below 4 GeV/c^2 in m_{A}. Similarly, charged Higgs bosons, although kinematically accessible with a mass between 57 and 82 GeV/c^2, have a large branching fraction into W*A in this region. As our charged Higgs boson searches in these channels assume m_{A} above 12 GeV/c^2 (see Table 1), the overall experimental sensitivity in these regions remains weak and no exclusion at 95% CL can be derived, in agreement with the expected performance. The largest value of CL$_{\mathrm{s}}$ is 7% in the unexcluded region around 12 GeV/c^2 in m_{A} and 33% in the unexcluded hole below 4 GeV/c^2. Note that the nearby region with m_{h} from 82 GeV/c^2 to the theoretical upper bound on m_{h} is excluded

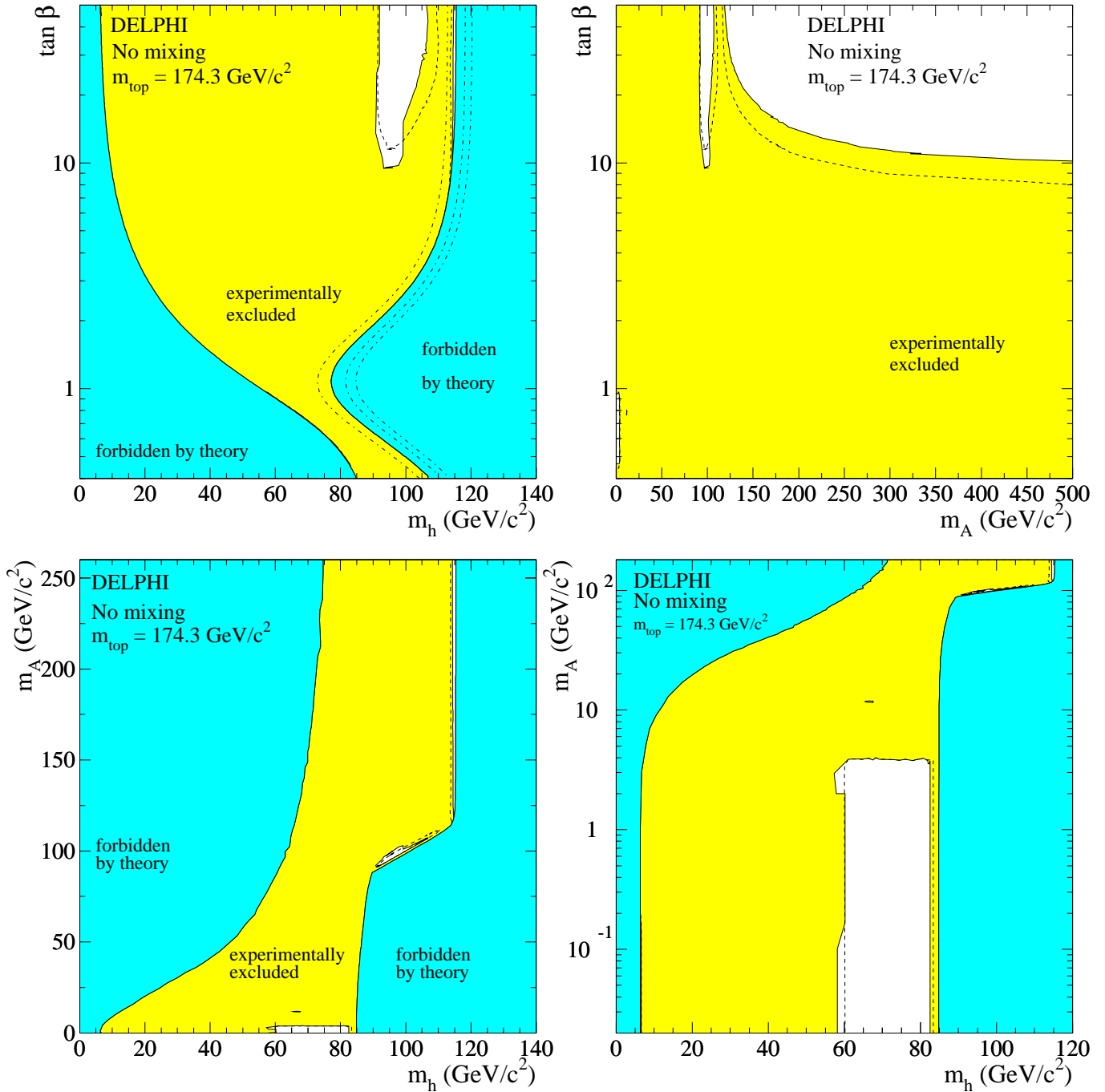Figure 9: MSSM no mixing scenario for a top mass of 174.3 GeV/c^2: regions excluded at 95% CL by combining the results of the Higgs boson searches in the whole DELPHI data sample (light-grey). Among the three unexcluded regions at low m_A, the strip at low m_h is fully excluded by the limit on the Z partial width that would be due to new physics [35]. The dashed curves show the median expected limits. The medium-grey areas are the regions not allowed by theory. The dash-dotted lines in the top left-hand plot are the theoretical upper bounds for a top mass of 169.2, 179.4 and 183.0 GeV/c^2 (from left to right).

at 95% CL by the charged Higgs boson searches through their fermionic decays which dominate the W*A mode there.

The above results establish the following 95% CL lower limits on m_h and m_A for $m_{top} = 174.3$ GeV/c^2:

$$m_h > 90.7 \text{ GeV}/c^2 \qquad m_A > 91.2 \text{ GeV}/c^2$$

for any value of $\tan\beta$ between 1.0 and 50. The expected median limits are 91.1 GeV/c^2 for both m_h and m_A. The observed limits in m_A and m_h are reached at $\tan\beta$ around 15, in a region where both the hZ and hA processes contribute. For $m_{top} = 174.3$ GeV/c^2, two ranges in $\tan\beta$ are excluded for any value of m_A between 0.02 and 1000 GeV/c^2, the largest interval being between 1.0 and 9.7 (expected [0.9-7.7]).

The m_{top} dependence of the above limits was studied, as shown in Table 5 and Fig. 14. In this scenario, both the mass limits and the excluded range in $\tan\beta$ change when varying m_{top}. Indeed, as already mentioned, the mass limits in m_A and m_h rely on the searches for H, whose mass is very sensitive to m_{top} in the region where the limits are set. Similarly, the maximal value of m_h, which governs the limits in $\tan\beta$, is reached at large m_A where m_h is very sensitive to m_{top} (see Table 4). Note that for a top mass of 169 GeV/c^2, m_H decreases by 3 GeV/c^2 in the region where the mass limits are set, making the H signal more within the sensitivity of LEP2: the whole parameter space of the no mixing scenario is then accessible and found to be excluded at 95% CL, apart from two holes at $\tan\beta$ below 1.0, one at m_A around 12 GeV/c^2, which is excluded at 92% CL, and a larger one below 4 GeV/c^2, which is disfavoured at 69% CL only.

5.4 The no mixing scenario but with positive μ and large M_{susy}

The excluded regions in the no mixing scenario with positive μ and large M$_{susy}$ are presented in Fig. 10 for a top mass value of 174.3 GeV/c^2. The larger M_{susy} makes the impact of the H signal, and hence the exclusion limits, weaker than in the previous scenario. On the other hand, the results in the low mass region, at m_A below 12 GeV/c^2, are similar to those in the no mixing scenario. The direct searches leave a tiny unexcluded strip at low m_h and very low m_A which is excluded by the limit on Γ^{new}. Three other regions, at m_h between 56 and 72 GeV/c^2, remain unexcluded even when charged Higgs boson searches are included, due to the large branching fraction into W*A decays, which are not covered by these searches at such low A masses. The holes around 8 and 12 GeV/c^2 in m_A are however excluded at 93% and 91% CL, respectively, while the larger area below 4 GeV/c^2 in m_A is disfavoured at 60% CL only.

The above results establish the following 95% CL lower limits on m_h and m_A for $m_{top} = 174.3$ GeV/c^2:

$$m_h > 89.8 \text{ GeV}/c^2 \qquad m_A > 90.6 \text{ GeV}/c^2$$

for any value of $\tan\beta$ between 1.0 and 50. The expected median limits are 90.5 GeV/c^2 for m_h and 90.6 GeV/c^2 m_A. For $m_{top} = 174.3$ GeV/c^2 the range in $\tan\beta$ between 1.0 and 4.5 (expected [1.0-4.3]) is excluded for any value of m_A between 0.02 and 1000 GeV/c^2.

The m_{top} dependence of the above limits is presented in Table 5 and Fig. 14. The mass limits vary only slightly with m_{top}, since in the region where these are set, m_h is insensitive to m_{top} while m_H, although sensitive to m_{top}, is very close to the kinematic limit. Contrary to the case of the no mixing scenario, the parameter space of this scenario does not become fully accessible for a top mass of 169 GeV/c^2, due to too high an upper
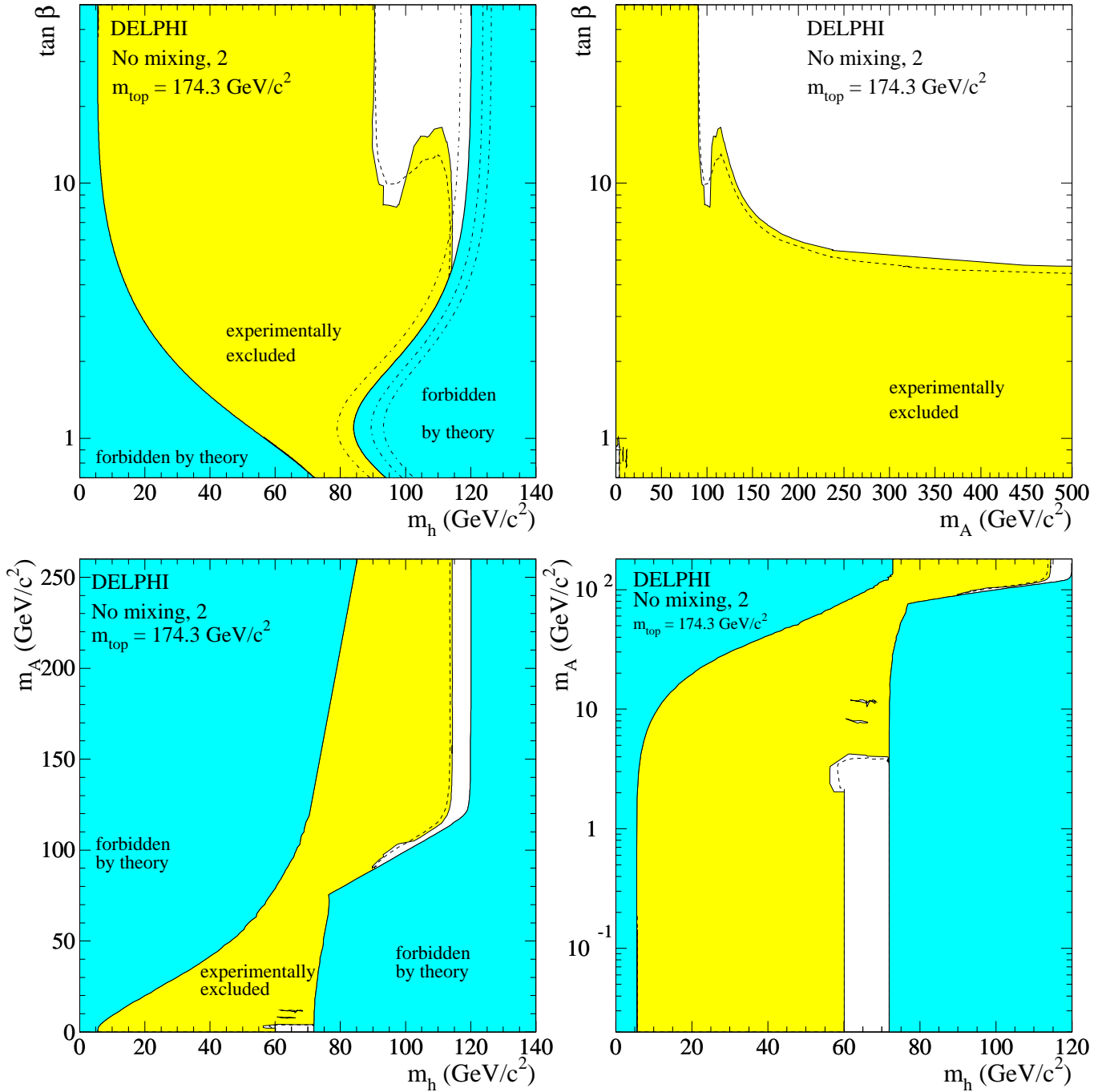
Figure 10: MSSM no mixing scenario with positive μ and large M_{susy} for a top mass of 174.3 GeV/c^2: regions excluded at 95% CL by combining the results of the Higgs boson searches in the whole DELPHI data sample (light-grey). Among the four unexcluded regions at low m_A, the strip at low m_h is fully excluded by the limit on the Z partial width that would be due to new physics [35]. The dashed curves show the median expected limits. The medium-grey areas are the regions not allowed by theory. The dash-dotted lines in the top left-hand plot are the theoretical upper bounds for a top mass of 169.2, 179.4 and 183.0 GeV/c^2 (from left to right).

(resp. lower) bound on m_{h} (resp. m_{H}). The exclusion is thus much weaker than in the no mixing scheme but stronger than in the $m_{\mathrm{h}}^{\mathrm{max}}$ scenarios.

5.5 The large μ scenario

The excluded regions in the large μ scenario are presented in the $(m_{\mathrm{h}}, \tan\beta)$ and $(m_{\mathrm{A}}, \tan\beta)$ planes in Fig. 11 for values of the top quark mass of 174.3 and 179.4 GeV/c^2. In these figures, the contribution of the H signal and that of the searches for neutral Higgs bosons decaying into hadrons of any flavour are highlighted.

A large fraction of the allowed domain is excluded by the searches for the h, A and H Higgs bosons into standard MSSM final states. In particular, since the theoretical upper bound on the h boson mass in this scenario is low (around 110.0 GeV/c^2, see Table 4), the sensitivity of the hZ channels is high even at large $\tan\beta$, which explains why the excluded region reaches the theoretically forbidden area for large values of $\tan\beta$. As the value of the upper bound on m_{h} is also the theoretical lower bound on m_{H} at large $\tan\beta$, allowing for the production of H translates into a significant gain in exclusion, namely at $\tan\beta$ above 8. The searches for neutral Higgs bosons decaying into hadrons of any flavour bring an additional exclusion in regions left unexcluded by the standard searches at $\tan\beta$ around 14. At moderate m_{A}, hZ and hA productions are low due to weak hZZ couplings for hZ and to kinematics for hA. On the other hand, HZ production is large but H is decoupled from b$\bar{\mathrm{b}}$. At larger m_{A}, hA and HZ productions are kinematically forbidden, hZ production is large but the h$\to$b$\bar{\mathrm{b}}$ branching fraction vanishes. In both cases, the Higgs boson whose production is allowed (H or h) has a large branching fraction into hadrons and a mass close to the sensitivity of our searches for a neutral Higgs boson decaying into hadrons and fully coupled to the Z. This explains why these searches lead to an additional but only partial exclusion in these regions. Note that increasing the top quark mass from 174.3 to 179.4 GeV/c^2 leads to a larger unexcluded area. There are indeed more points with vanishing h or H branching fractions into b$\bar{\mathrm{b}}$ and, as m_{h} and m_{H} increase with m_{top}, the impact of the searches for hadronically decaying Higgs bosons also becomes weaker. However, when combining the four LEP experiments, the sensitivity of these searches increases and becomes high enough to cover almost entirely these regions of vanishing branching fractions into b$\bar{\mathrm{b}}$ [7].

Below 3 GeV/c^2 in m_{A}, the direct searches leave two unexcluded holes at $\tan\beta$ around 1. The one at $\tan\beta$ above 1 is fully excluded by the limit on Γ^{new} for either value of m_{top}. The hole at $\tan\beta$ below 1 remains unexcluded. The largest value of $\mathrm{CL_s}$ in this area is 12% for $m_{\mathrm{top}} = 174.3$ GeV/c and 6% for $m_{\mathrm{top}} = 179.4$ GeV/c.

The above results establish the following 95% CL lower limits on m_{h} and m_{A} for $m_{\mathrm{top}} = 174.3$ GeV/c^2:

$$m_{\mathrm{h}} > 94.2 \text{ GeV}/c^2 \qquad m_{\mathrm{A}} > 96.6 \text{ GeV}/c^2$$

for any value of $\tan\beta$ between 0.9 and 50. The expected median limits are 90.3 GeV/c^2 for m_{h} and 92.8 GeV/c^2 for m_{A}. The observed limits in m_{A} and m_{h} are reached at $\tan\beta$ around 14, in a region where the hZ, HZ and hA processes contribute. For $m_{\mathrm{top}} = 174.3$ GeV/c^2, two ranges in $\tan\beta$ are excluded for any value of m_{A} between 0.02 and 1000 GeV/c^2, the largest interval being between 0.9 and 13.7 (expected [0.9-12.9]).

The m_{top} dependence of the above limits is presented in Table 5 and Fig. 14. Except for $m_{\mathrm{top}} = 174.3$ GeV/c^2, the mass limits vary only slightly with m_{top} and are in agreement with the expected ones. The difference at $m_{\mathrm{top}} = 174.3$ GeV/c^2 has been
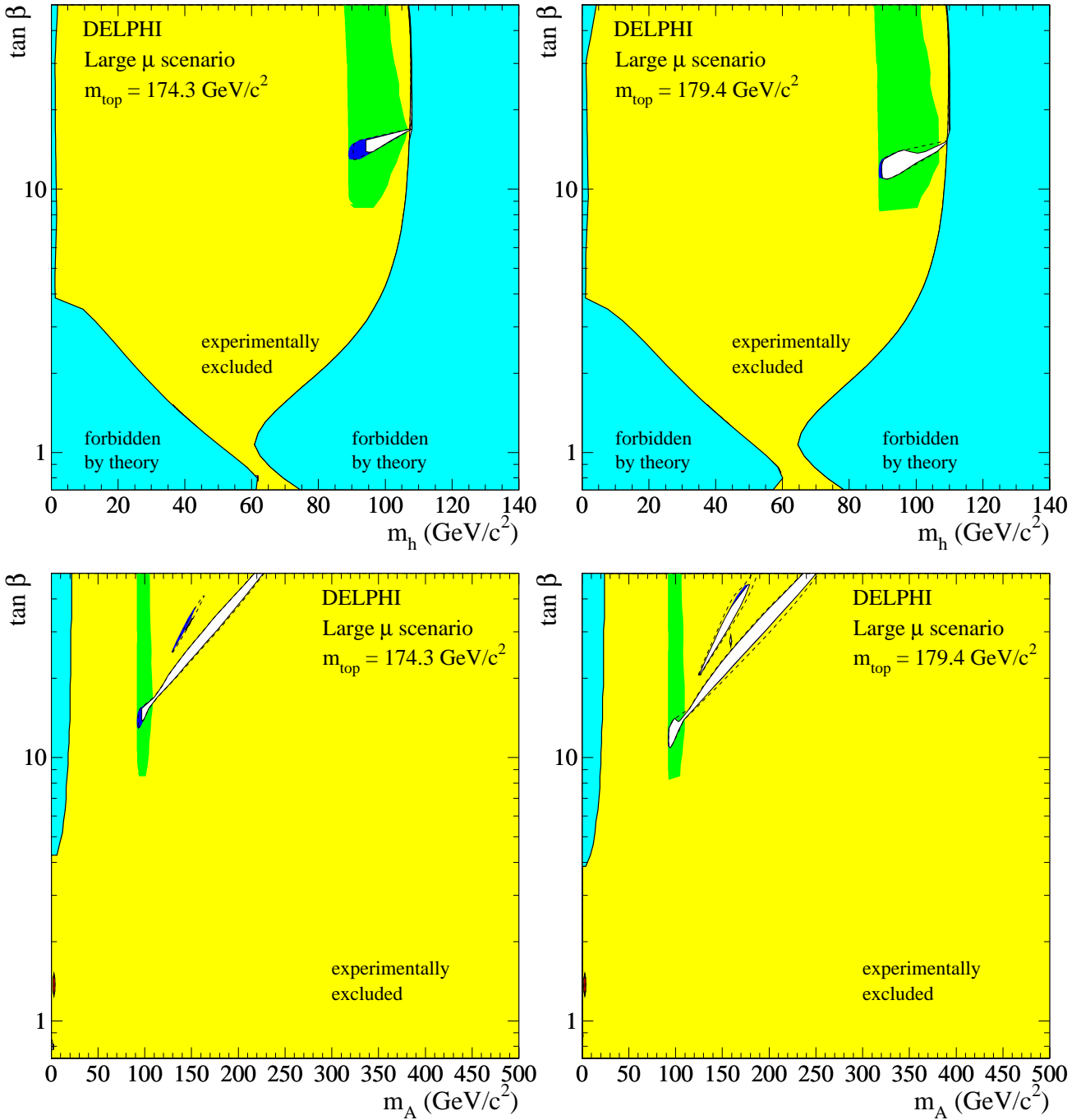
Figure 11: MSSM large μ scenario: regions excluded at 95% CL by combining the results of the Higgs boson searches in the whole DELPHI data sample (light-grey area and embedded domains in medium- and dark-grey). Results are shown for two values of the top mass, 174.3 and 179.4 GeV/c^2. The domains embedded in the light-grey area at large $\tan\beta$ are excluded by the searches for the heavy scalar Higgs boson, H (medium-grey or green) and by the flavour-blind searches (dark-grey or dark-blue). Of the two unexcluded holes at low m_A, the one at $\tan\beta$ above 1 is excluded by the limit on the Z partial width [35] that would be due to new physics. The dashed curves show the median expected limits. The medium-grey areas with bold contours are the regions not allowed by theory. Note in particular the large region forbidden at low m_A in the (m_A, $\tan\beta$) projections, which is due to points leading to unphysical h masses.

traced back to the deficit in data with respect to background expectations which was observed in the flavour-blind searches applied to the Higgsstrahlung process [22] when testing masses above 100 GeV/c^2, which corresponds to the range of m_H values in the region where the mass limits are obtained in the large μ scenario. In this region, the set of independent channels which are selected to be statistically combined (see Sec. 3.3) varies strongly from one top mass value to the other, due to still large H branching fractions into b$\bar{\text{b}}$ at $m_{\text{top}} = 169.2$ GeV/c^2 and to m_H values increasing with m_{top} (see Table 4). At $m_{\text{top}} = 174.3$ GeV/c^2, the weight of the flavour-blind HZ searches is maximal and the deficit in data of these searches translates into a difference between the observed and median limits.

5.6 The gluophobic scenario

For the gluophobic scenario the excluded regions in the $(m_h, \tan\beta)$, $(m_A, \tan\beta)$ and (m_h, m_A) planes are presented in Fig. 12 for a top mass value of 174.3 GeV/c^2. Although this scenario was designed to test Higgs boson searches at hadron colliders, with a phenomenology very different from that of LEP, results are similar to those derived in the previous scenarios. The exclusion is defined by the results in the hZ (hA) channels in the low (large) $\tan\beta$ region while they both contribute at intermediate values. The direct searches leave several unexcluded holes below 4 GeV/c^2 in m_A and at $\tan\beta$ below 2, which are all excluded by the limit on Γ^{new}.

The above results establish the following 95% CL lower limits on m_h and m_A for $m_{\text{top}} = 174.3$ GeV/c^2:

$$m_h > 87.0 \text{ GeV}/c^2 \qquad m_A > 92.9 \text{ GeV}/c^2$$

for any value of $\tan\beta$ between 0.4 and 50. The expected median limits are 87.0 GeV/c^2 for m_h and 93.0 GeV/c^2 for m_A. The observed limits in m_A and m_h are reached at $\tan\beta$ around 50, in a region where only the hA process contributes. Contrary to the other scenarios, the h and A bosons are not degenerate in mass at large $\tan\beta$, which reflects in the significant difference between the h and A mass limits. For $m_{\text{top}} = 174.3$ GeV/c^2, the range in $\tan\beta$ between 0.4 and 5.2 (expected [0.4-4.8]) is excluded for any value of m_A between 0.02 and 1000 GeV/c^2.

The m_{top} dependence of the above limits is shown in Table 5 and Fig. 14. As already mentioned, the h and A bosons are not degenerate at large $\tan\beta$ and moderate m_A, the region where the mass limits are set. As a consequence, the value of m_h at fixed m_A and $\tan\beta$ is observed to vary significantly with m_{top} in that region. This is the main reason for the variations of the mass limits with m_{top}, an additional effect being the variations of m_H which is kinematically accessible at low m_{top} in this scenario (see Table 4). On the other hand, the variation of the excluded range in $\tan\beta$ is due, as in the other scenarios, to the change in the maximal value of m_h which is very sensitive to m_{top}.

5.7 The small α scenario

The excluded regions in the small α scenario are presented in Fig. 13 for a top mass value of 174.3 GeV/c^2. The small α scheme is the second example of a scenario aiming at testing potentially difficult cases for the Higgs boson searches at hadron colliders. As mentioned in section 4, this scenario presents regions of the parameter space where the h $\rightarrow$ b$\bar{\text{b}}$ and h $\rightarrow \tau^+\tau^-$ decays vanish, which could be a problem at LEP too. The results in Fig. 13, similar to those derived in the previous scenarios, show that this is not the case.
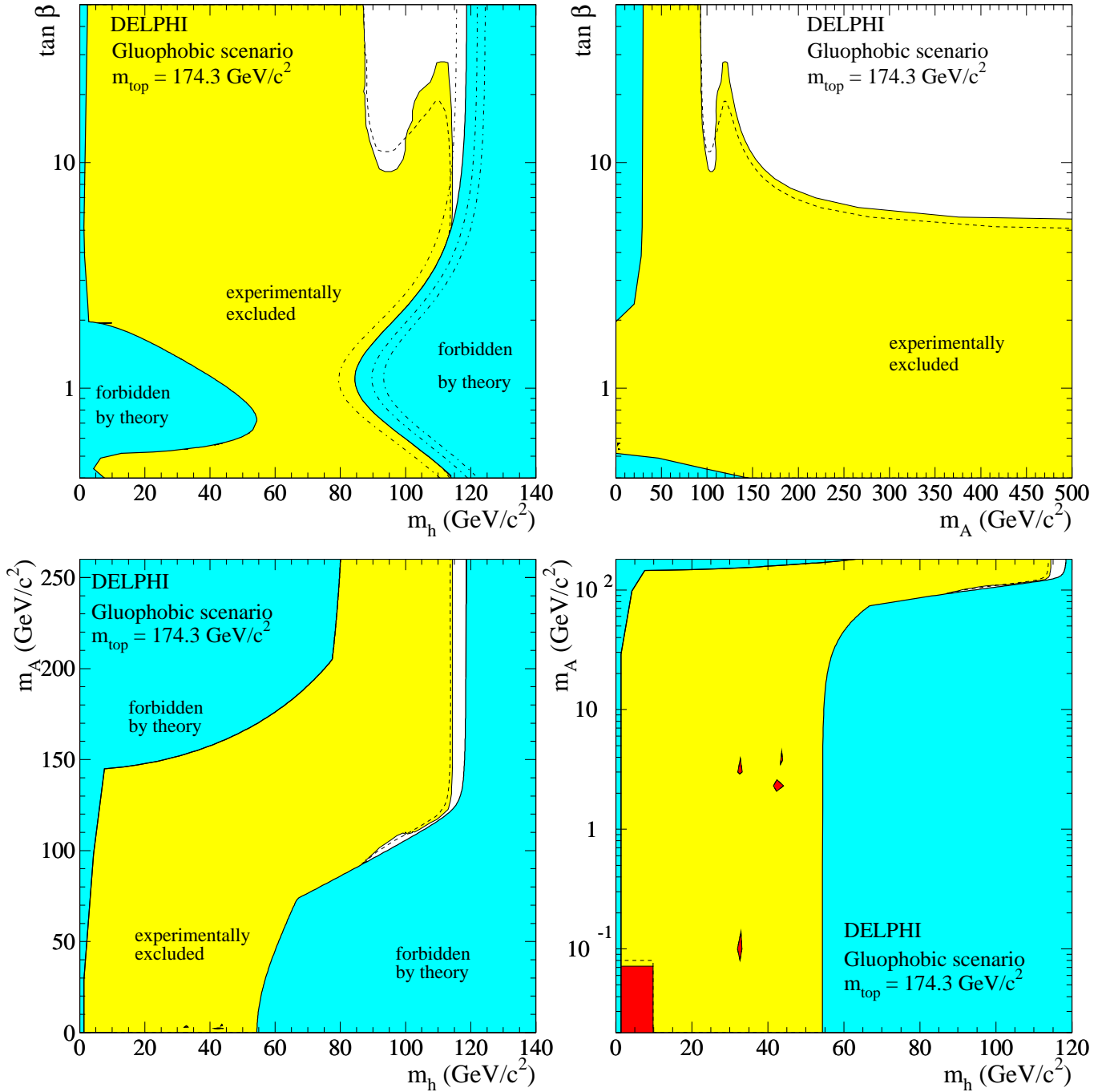
Figure 12: MSSM gluophobic scenario for a top mass of 174.3 GeV/c^2: regions excluded at 95% CL by combining the results of the Higgs boson searches in the whole DELPHI data sample (light-grey). The unexcluded holes at low m_A are fully excluded by the limit on the Z partial width [35] that would be due to new physics (dark-grey). The dashed curves show the median expected limits. The medium-grey areas are the regions not allowed by theory. Note in particular the large forbidden region in the $(m_A, \tan\beta)$ projection, which is due to points leading to unphysical h masses. The dash-dotted lines in the top left-hand plot are the theoretical upper bounds for a top mass of 169.2, 179.4 and 183.0 GeV/c^2 (from left to right).
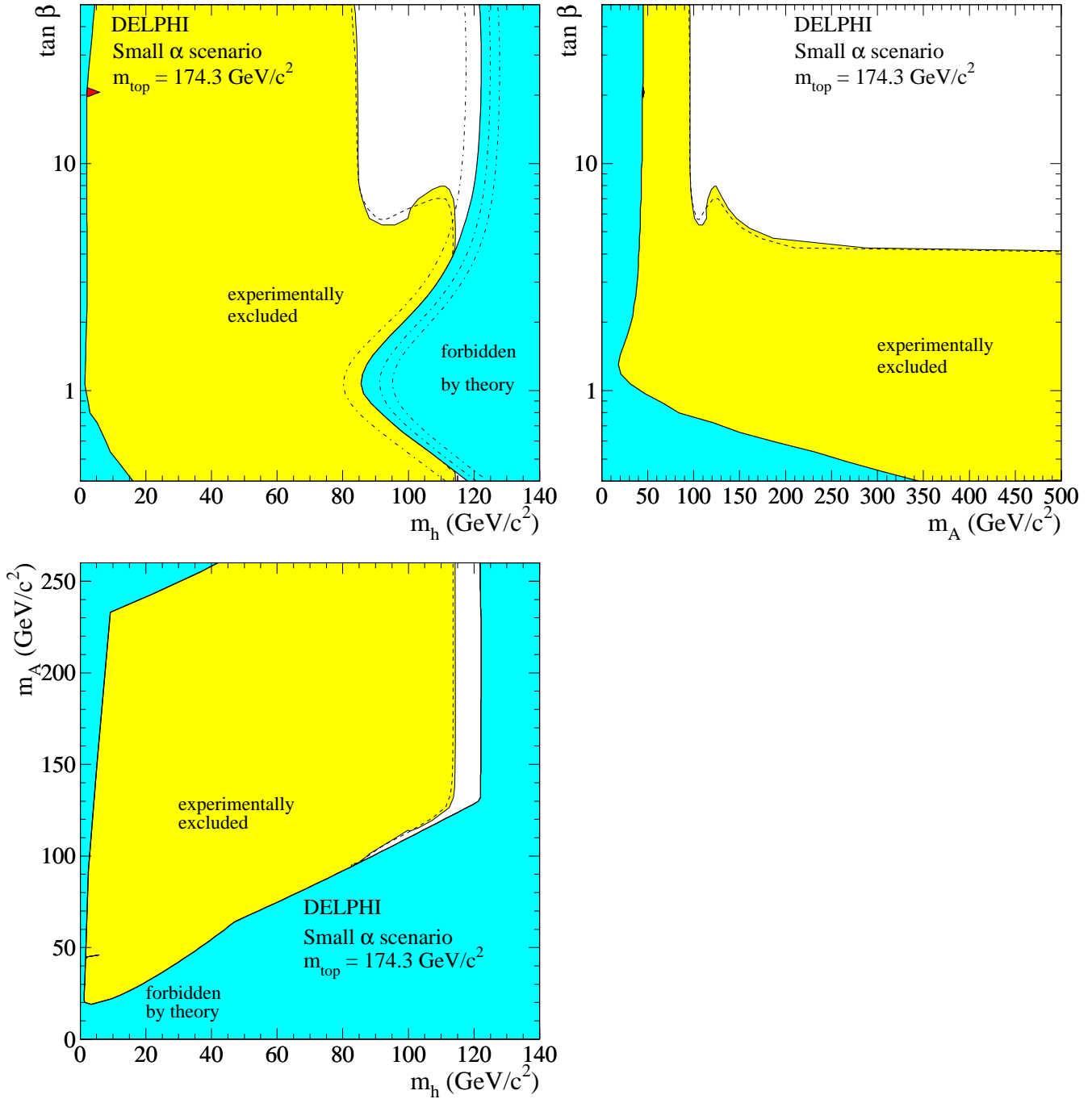
Figure 13: MSSM small α scenario for a top mass of 174.3 GeV/c^2: regions excluded at 95% CL by combining the results of the Higgs boson searches in the whole DELPHI data sample (light-grey). There is one unexcluded hole at low m_h and $\tan\beta$ around 20 which is excluded by the limit on the Z partial width [35] that would be due to new physics (dark-grey). The dashed curves show the median expected limits. The medium-grey areas are the regions not allowed by theory. Note in particular the large forbidden region in the $(m_A, \tan\beta)$ projection, which is due to points leading to unphysical h masses. The dash-dotted lines in the top left-hand plot are the theoretical upper bounds for a top mass of 169.2, 179.4 and 183.0 GeV/c^2 (from left to right).

At large $\tan\beta$, in the region accessible at LEP, the $h \to b\bar{b}$ branching fraction, although reduced, remains high enough (e.g. above 70% in the region where the mass limits are set) to ensure a good sensitivity. At low m_h, the direct searches leave one unexcluded island that is fully excluded by the limit on Γ^{new}.

The above results establish the following 95% CL lower limits on m_h and m_A for $m_{\text{top}} = 174.3$ GeV/c^2:

$$m_h > 83.5 \text{ GeV}/c^2 \qquad m_A > 95.8 \text{ GeV}/c^2$$

for any value of $\tan\beta$ between 0.4 and 50. The expected median limits are 82.6 GeV/c^2 for m_h and 95.0 GeV/c^2 for m_A. The observed limits in m_A and m_h are reached at $\tan\beta$ around 50, in a region where only the hA process contributes. As in the previous scenario, the h and A bosons are not degenerate in mass at large $\tan\beta$, which reflects in the significant difference between the h and A mass limits. For $m_{\text{top}} = 174.3$ GeV/c^2, the range in $\tan\beta$ between 0.4 and 4.0 (expected [0.5-3.9]) is excluded for any value of m_A between 0.02 and 1000 GeV/c^2.

The m_{top} dependence of the above limits is shown in Table 5 and Fig. 14. As in the previous scenario, the value of m_h at fixed m_A and $\tan\beta$ varies significantly with m_{top} in the region where the mass limits are set, which explains the variations of the latter. The H signal, being kinematically inaccessible for most values of m_{top} (see Table 4) plays no role in this scenario. Finally, the variation of the excluded range in $\tan\beta$ is due to the change in the maximal value of m_h which is very sensitive to m_{top}.

5.8   Summary

The lower bounds in mass and excluded ranges in $\tan\beta$ obtained in the eight CP-conserving benchmark scenarios presented in the previous sections are summarized in Table 5. The variation with m_{top} of the excluded ranges in $\tan\beta$ is further illustrated in Fig. 14. All lower bounds in mass are at the 95% CL, as well as each individual (either lower or upper) bound in $\tan\beta$. In all scenarios, the radiative corrections on the Higgs boson masses and couplings have been computed in the Feynman-diagrammatic approach with all dominant two-loop order terms included, using version 2.0 of the FeynHiggs code [30].

scenario	limits	m_{top} (GeV/c^2)			
		169.2	174.3	179.4	183.0
$m_{\mathrm{h}}^{\max}$	m_{h}	89.7	89.7	89.7	89.6
	m_{A}	90.4	90.4	90.4	90.4
	$\tan\beta$	0.59 - 2.46	0.72 - 1.96	0.93 - 1.46	none
$m_{\mathrm{h}}^{\max}$	m_{h}	89.6	89.6	89.5	89.6
$\mu > 0$	m_{A}	90.3	90.3	90.3	90.3
	$\tan\beta$	0.59 - 2.61	0.71 - 2.00	0.87 - 1.54	none
$m_{\mathrm{h}}^{\max}$	m_{h}	89.6	89.6	89.5	89.6
$\mu > 0, \mathrm{X_t} < 0$	m_{A}	90.5	90.4	90.4	90.4
	$\tan\beta$	0.53 - 3.20	0.63 - 2.46	0.72 - 1.96	0.84 - 1.63
no mixing	m_{h}	112.8	90.7	90.0	89.9
	m_{A}	1000.	91.2	90.8	90.5
	$\tan\beta$	0.40 - 50.0	0.40 - 9.70	0.40 - 5.40	0.40 - 4.40
	$\tan\beta, m_{\mathrm{A}} > 12.0$	0.46 - 0.96	0.46 - 0.96	0.47 - 0.97	0.47 - 0.97
no mixing	m_{h}	89.9	89.8	89.7	89.8
$\mu > 0$	m_{A}	90.8	90.6	90.4	90.3
large $\mathrm{M_{SUSY}}$	$\tan\beta$	0.70 - 6.95	0.70 - 4.55	0.70 - 3.43	0.70 - 2.97
	$\tan\beta, m_{\mathrm{A}} > 12.0$	0.70 - 1.01	0.70 - 1.01	0.70 - 1.02	0.70 - 1.01
Large μ	m_{h}	90.2	94.2	89.7	89.3
	m_{A}	92.5	96.6	92.6	92.5
	$\tan\beta$	0.72 - 14.79	0.72 - 13.68	0.72 - 10.91	0.72 - 10.63
	$\tan\beta, m_{\mathrm{A}} > 2.4$	0.72 - 0.79	0.75 - 0.85	0.86 - 0.90	none
Gluophobic	m_{h}	87.8	87.0	86.4	86.2
	m_{A}	93.0	92.9	93.2	93.5
	$\tan\beta$	0.40 - 9.70	0.42 - 5.22	0.48 - 3.76	0.51 - 3.19
Small α	m_{h}	84.3	83.5	82.5	82.0
	m_{A}	95.0	95.8	96.5	97.2
	$\tan\beta$	0.40 - 5.97	0.43 - 4.03	0.52 - 3.12	0.55 - 2.69

Table 5: 95% CL lower bounds on m_{h} and m_{A} in GeV/c^2 and excluded ranges in $\tan\beta$ obtained in the different MSSM CP-conserving benchmark scenarios, as a function of m_{top}. Except for the two no mixing and the large μ scenarios, the exclusions in mass are valid for all values of $\tan\beta$ between 0.4 and 50, and the exclusions in $\tan\beta$ hold for all values of m_{A} between 0.02 and 1000 GeV/c^2. In the three other scenarios, part of the interval in $\tan\beta$ is excluded only for m_{A} above a few GeV/c^2 threshold: this sub-interval is indicated in a fourth line together with the threshold in m_{A}. As a consequence, the mass bounds in these scenarios are valid only for values of $\tan\beta$ outside the quoted sub-interval.
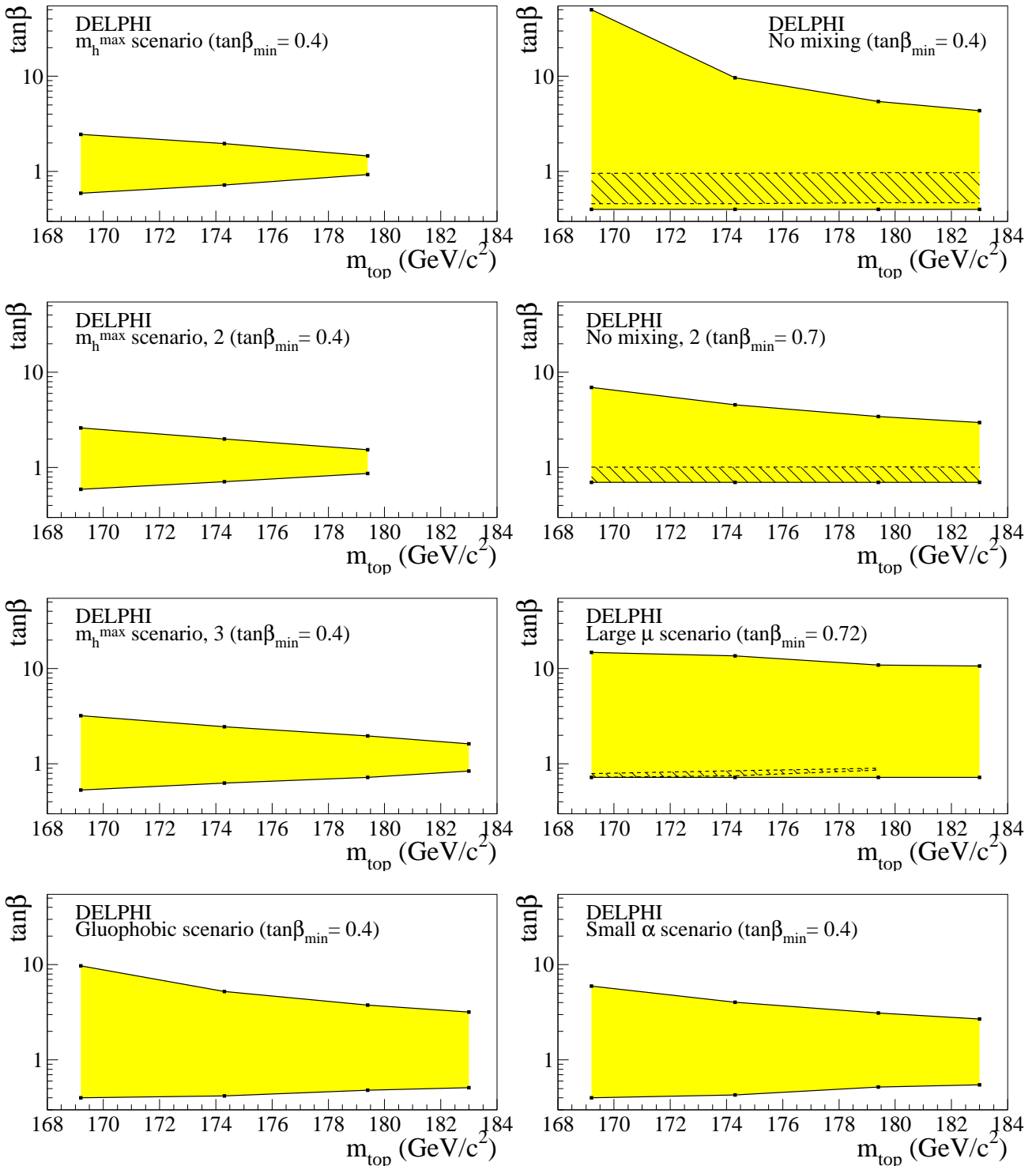
Figure 14: Variation with m_{top} of the ranges in $\tan\beta$ excluded by DELPHI in the CP-conserving MSSM benchmark scenarios. Note that each bound in $\tan\beta$ is a limit (either upper or lower) at 95% CL. These bounds hold for the whole interval of m_A between 0.02 and 1000 GeV/c^2, except in the hatched intervals, where the exclusion is valid above 12 GeV/c^2 in the two no mixing scenarios and above 2.4 GeV/c^2 in the large μ scenario.

6 The CP-violating MSSM scenarios

In most of the parameter space of the CP-violating MSSM scenarios studied in this paper, only the two lightest neutral Higgs bosons, H_1 and H_2 are kinematically accessible at LEP energies. If their couplings to the Z boson are not strongly suppressed by CP-violation, the main production processes are the H_1Z, H_2Z and H_1H_2 processes, with H_1Z dominating at low $\tan\beta$, H_1H_2 at large $\tan\beta$ and H_2Z contributing over the whole range of $\tan\beta$ values allowed in each scenario. In restricted areas of the parameter space, the second pair-production process, H_1H_3, can add a non-negligible signal and has also been considered in the searches. On the other hand, in most scenarios, charged Higgs bosons have a mass above 100 GeV/c^2, and thus have not been included.

As already mentioned, CP violation in the MSSM Higgs sector is introduced through radiative corrections. Besides the two parameters used to define the scenarios at tree level, chosen as $\tan\beta$ and $m_{H^\pm}$, radiative corrections introduce additional parameters. As in the CP-conserving case, these are primarily m_{top} and the set of parameters related to supersymmetry breaking: μ, M_{susy}, M_2, $m_{\tilde{g}}$ and A, as defined in section 4 [2,28]. In addition, CP violation introduces phases. The unification assumptions made for the supersymmetry breaking parameters, and the global symmetries that govern the dimension-four operators of the MSSM Lagrangian, can be used to reduce the number of CP-violating phases to only two [37]. In the scenarios studied hereafter, these phases are taken as the phase of the gluino mass, $\arg(m_{\tilde{g}})$ and the phase of the common stop and sbottom trilinear coupling, $\arg(A)$.

6.1 The benchmark scenarios

The dominant CP-violating effects on the neutral Higgs boson masses and couplings to gauge bosons are proportional to

$$\frac{m_{top}^4}{v^2}\frac{Im(\mu A)}{M_{susy}^2}$$

where v^2 is the quadratic sum of the vacuum expectation values of the two Higgs field doublets [38]. Sizeable effects are thus expected for moderate values of M_{susy}, large values of μ and phases $\arg(A)$ around 90°. A strong dependence on the value of m_{top} is also to be expected.

Along these lines, Ref. [38] proposed a benchmark scenario with maximal CP-violation, the CPX scenario, as an appropriate scheme for direct searches at LEP and other colliders. The values of its underlying parameters are quoted in Table 6. As expected from the above discussion, the value of M_{susy}, a few hundred GeV/c^2, is moderate, μ and $|A|$ take large values, 2 and 1 TeV/c^2 respectively, and the CP-violating phase $\arg(A)$ is set at 90°. Although the gluino-mass phase has a small impact on the CP-violating effects, these appear to be reinforced at 90° [37], a value which was thus retained for $\arg(m_{\tilde{g}})$. The values listed in Table 6 fulfill the existing constraints from measurements of the electron and neutron electric dipole moments, by making the first two generations of squarks sufficiently heavy, with masses above 1 TeV/c^2. In the following, the CPX scenario has been studied for four values of the top quark mass, $m_{\text{top}} = 169.2$, 174.3, 179.4 and 183.0 GeV/c^2.

In addition to the CPX scenario, a few variants have also been considered in order to study the dependence of the CP-violation effects on the values of phases, μ and M_{susy}. The values tested are quoted in Table 6. The two CP-violating phases, still taken to be

scenario	M_{susy} (GeV/c^2)	M_2 (GeV/c^2)	$|m_{\tilde{g}}|$ (GeV/c^2)	μ (GeV/c^2)	$|A|$ (GeV/c^2)	arg($m_{\tilde{g}}$)=arg(A) (degrees)
CPX	500	200	1000	2000	1000	90
phase study	500	200	1000	2000	1000	0,30,60,135,180
μ study	500	200	1000	500,1000,4000	1000	90
M_{susy} =1 TeV/c^2	1000	200	1000	2000	1000	90
M_{susy} =1 TeV/c^2, scaled	1000	200	2000	4000	2000	90

Table 6: Values of the underlying parameters for the representative CP-violating MSSM scenarios scanned in this paper, namely the CPX scenario and its ten variants.

equal, were varied from 0 to 180°, keeping all other parameters as in the CPX scenario. Values of μ below and above 2 TeV/c^2 were studied in the same way. Finally, the value of M_{susy} was increased from 500 GeV/c^2 to 1 TeV/c^2, keeping the phases at 90°, and either keeping all other parameters to their CPX values, or scaling the other parameters in such a way that the relation between $|m_{\tilde{g}}|$, $|A|$ and μ is as in the CPX scenario. In the following, these ten variants have been studied for $m_{\text{top}} = 174.3$ GeV/c^2 only.

In all scenarios, theoretical databases provided by the LEP Higgs working group were used [7]. In these, radiative corrections have been computed in two different approaches, the Feynman-diagrammatic approach of Ref. [30], already selected in the CP-conserving case (see Section 4), and the renormalization group approach of Ref. [39]. As in Section 4, the Feynman-diagrammatic calculations use version 2.0 of the FEYNHIGGS code. The renormalization group corrections rely on the CP-violating version CPH of the SUBHPOLE code.[3] Contrary to the CP-conserving case, where the calculations in the Feynman-diagrammatic approach were the most complete due to the inclusion of all dominant two-loop order terms, in the case of CP-violation neither of the two calculations can be preferred on theoretical grounds. Both contain one and two-loop corrections, but the CPH code has a more complete phase dependence at the two-loop order while FEYNHIGGS contains more corrections at the one-loop order with the full complex phase dependence and more corrections at the two-loop order but without the full phase dependence. This may result in large differences when convoluted with the experimental inputs. We thus present our results in the two frameworks separately. A comparison between the two calculations in the CP-conserving case can be found in Ref. [42].

The phenomenology of the three neutral Higgs bosons of the CP-violating MSSM is illustrated in Fig. 15 in the case of the CPX scenario for a top quark mass of 174.3 GeV/c^2, with radiative corrections computed in the renormalization group approach. The top figures show that the two lightest scalars, H_1 and H_2, are likely to be kinematically accessible at LEP2 in wide regions of the parameter space, in which their widths remain lower than 1 GeV/c^2, that is below the experimental resolution. The cross-section curves show that at low and large $\tan\beta$, the dominant production processes are the H_1Z and H_1H_2 processses, respectively, as in the CP-conserving case (see Fig. 4). On the other hand, at intermediate $\tan\beta$ and moderate m_{H_1}, the H_1Z cross-section is significantly weakened, as a result of the suppressed H_1ZZ coupling due to CP-violation. In the same region, the H_2Z process compensates only partly for this loss. Finally, the figures showing branching fractions compare the dominant H_1 and H_2 branching fractions for different values of $\tan\beta$. For all values of $\tan\beta$, decays into b$\bar{\text{b}}$ and $\tau^+\tau^-$ saturate the width of the lightest Higgs boson, H_1, in the mass range above the b$\bar{\text{b}}$ threshold up to the maximal sensitivity of LEP. In the same mass range, the second lightest Higgs boson, H_2, decays

---

[3]Since this work, updated versions of the two codes, CPSUPERH [40] and FEYNHIGGS 2.5 [41] have been made available. In both cases, the changes concern the Higgs boson decays and have no substantial impact on the phenomenology at LEP.
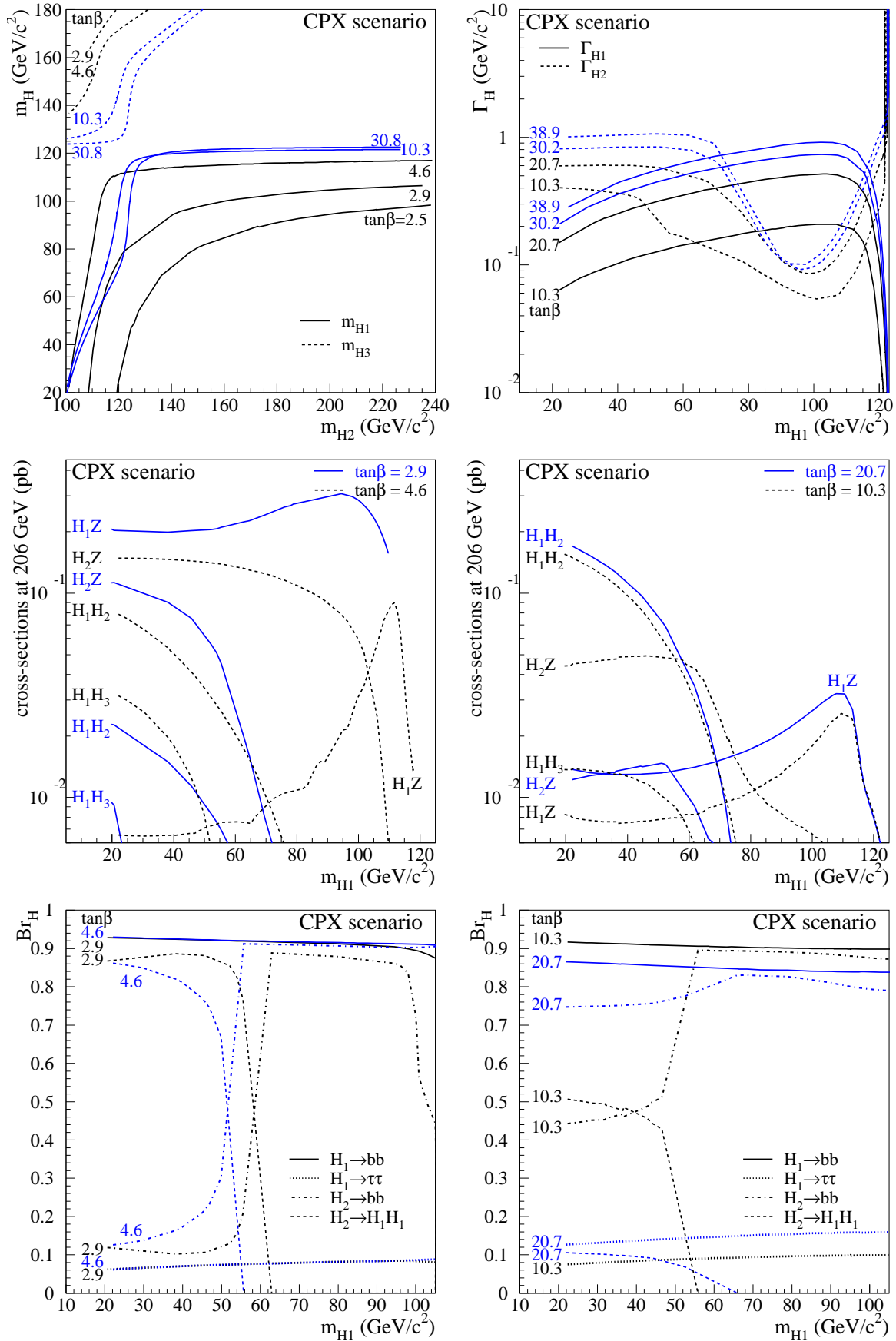
Figure 15: Properties of the three neutral Higgs bosons of the CP-violating MSSM in the CPX scenario with $m_{\text{top}} = 174.3$ GeV/c^2. Top: H_1, H_2 and H_3 masses and H_1, H_2 widths at various $\tan\beta$ values. Middle: production cross-sections at $\sqrt{s} = 206$ GeV, as a function of m_{H_1} and $\tan\beta$. Bottom: H_1 and H_2 dominant branching fractions as a function of m_{H_1} and $\tan\beta$. H_1 and H_2 decays into $b\bar{b}$ (solid and dash-dotted lines) are compared with H_1 decays into $\tau^+\tau^-$ (dotted lines) and H_2 decays into $H_1 H_1$ (dashed lines). The radiative corrections are as in Ref. [39].

predominantly into b$\bar{\text{b}}$ at large $\tan\beta$ only. At low and intermediate $\tan\beta$, the cascade decay H$_2 \to$ H$_1$H$_1$ dominates over the b$\bar{\text{b}}$ final state at masses up to 50 GeV/c^2 or so. A loss in experimental sensitivity can thus be anticipated in regions where the H$_1$Z cross-section is negligible and the H$_2$Z signals are not significant with respect to background, due to too weak H$_2$Z cross-sections or H$_2$ branching fractions into fermions.

6.2   Scan procedure

The scan procedure is similar to that described in Section 4.2 for the CP-conserving scenarios. The only changes are the following. The scan was performed over the MSSM parameters $\tan\beta$ and $m_{\text{H}^\pm}$. The range in $m_{\text{H}^\pm}$ spans from 4 GeV/c^2 up to 1 TeV/c^2. Values of $m_{\text{H}^\pm}$ below about 100 GeV/c^2 were noticed to give unphysical negative mass squared values in most scenarios and thus were removed from the scans. The range in $\tan\beta$ extends from the minimal value allowed in each scenario up to 40, a value above which the Higgs-bottom Yukawa coupling calculation becomes unreliable in the CP-violating MSSM scenarios. Theoretical points were generated randomly in both $\tan\beta$ and $m_{\text{H}^\pm}$ with a granularity which is sufficient to map the general features of the exclusion regions.

The signal expectations in each channel were then computed as outlined in Section 4.2, except for the width effects. In the CP-violating MSSM scans, the widths remain well below the experimental resolution for $\tan\beta$ up to 40 and m_{H_1} below 120 GeV/c^2 (see Fig. 15). Signal efficiencies and PDFs were thus exclusively determined from simulations with Higgs boson widths below 1 GeV/c^2.

7   Results in CP-violating MSSM scenarios

The regions of the MSSM parameter space excluded at 95% CL or more by combining the neutral Higgs boson searches of Table 1 are hereafter discussed in turn for each scenario. The additional constraint from the limit on the Z partial width that would be due to new physics [35] (used as described in Section 3.2 of [7]) brings no gain in sensitivity in any of the scenarios tested. Results are presented only in the (m_{H_1}, $\tan\beta$) plane, which is the only one relevant at LEP since the minimal values of m_{H_2} and $\tan\beta$ in most scenarios are such that the region accessible at LEP is much reduced in the other projections.

7.1   Dependence on the phases

The excluded regions in the (m_{H_1}, $\tan\beta$) plane for the CPX scenario and its variants with different phase values are presented in Fig. 16 for the renormalization group approach [39] and in Fig. 17 for the Feynman-diagrammatic calculations [30]. The top mass value is 174.3 GeV/c^2 in all plots.

Going from 0° to 180°, the excluded domain varies significantly. The qualitative trend, valid in the two theoretical approaches, is as follows. The extreme values (0° and 180°) correspond to scenarios with no CP violation, and hence to a large excluded region. Moreover, at 180°, the theoretically allowed region is reduced, especially at large $\tan\beta$ due to unphysical values of the Higgs-bottom Yukawa coupling. At phases between 60° and 135°, losses in sensitivity are observed at large $\tan\beta$ and m_{H_1} above 50 GeV/c^2, as well as in the intermediate $\tan\beta$ range for m_{H_1} below 60 GeV/c^2. This is the consequence of the
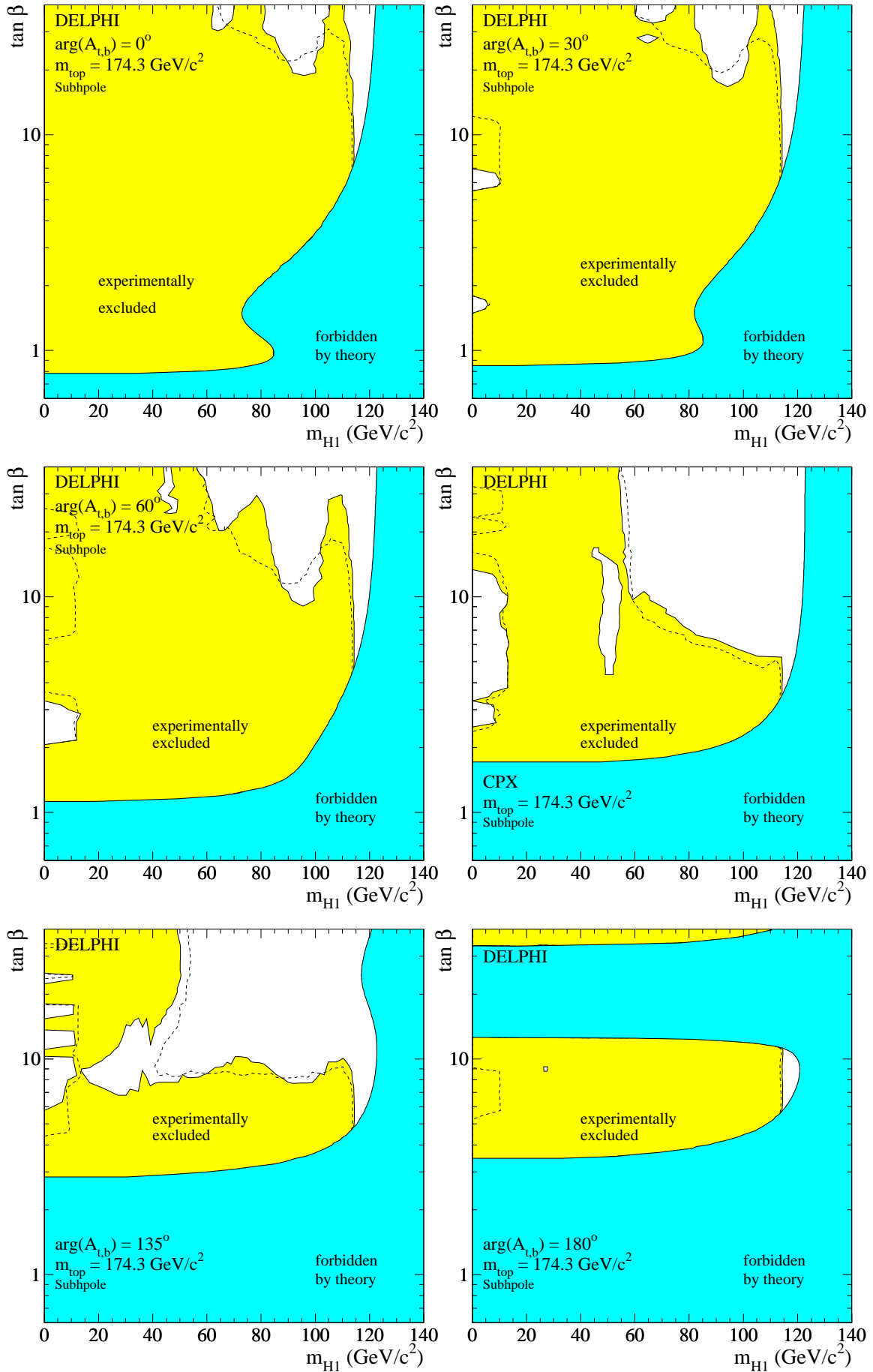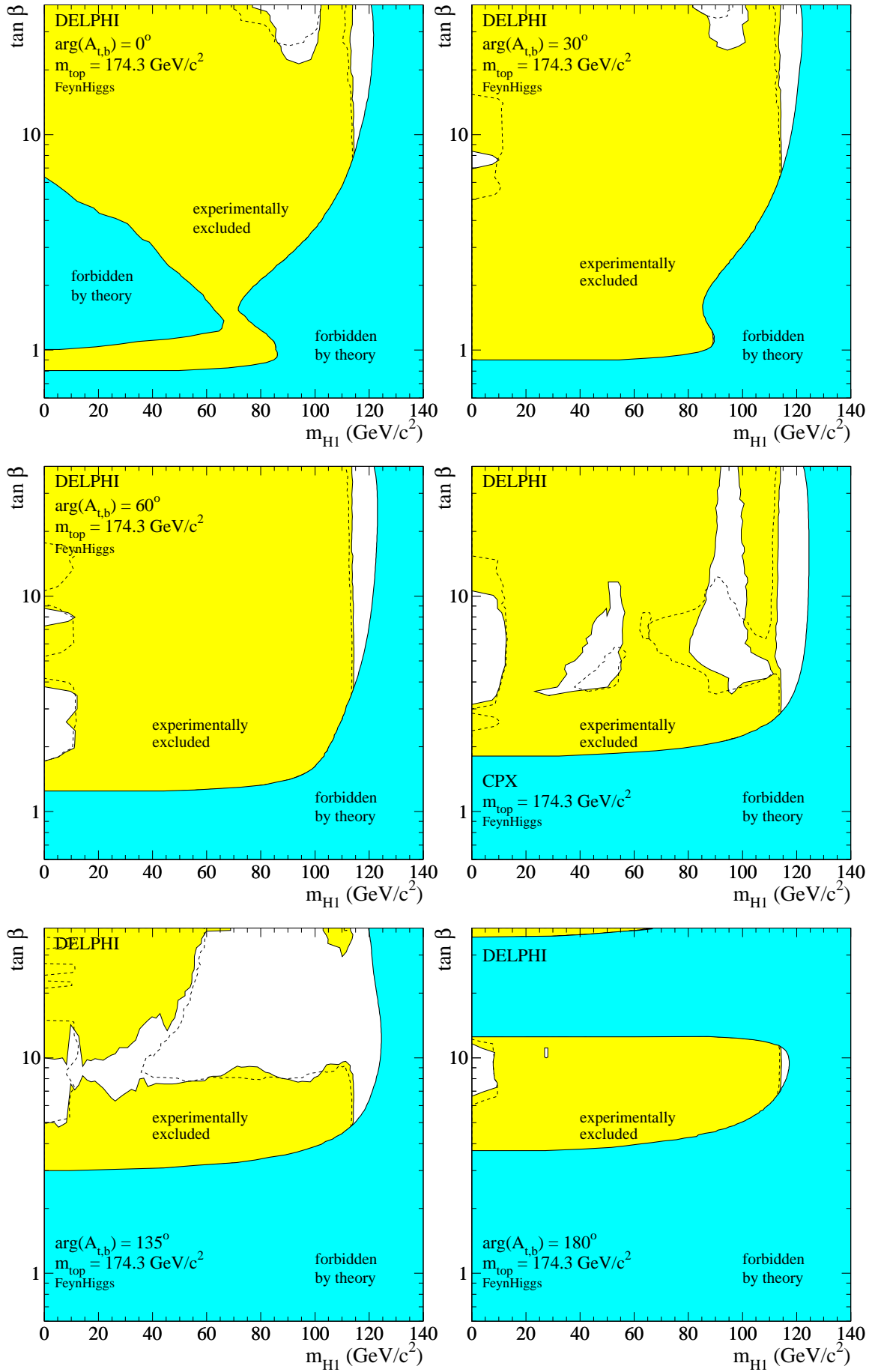
Figure 16: CP-violating MSSM scenarios with corrections as in Ref. [39] for different values of the phases: regions excluded at 95% CL by combining the results of the neutral Higgs boson searches in the whole DELPHI data sample (light-grey). The dashed curves show the median expected limits. The medium-grey areas are the regions not allowed by theory. The CPX scenario corresponds to phases of 90°.

Figure 17: CP-violating MSSM scenarios with corrections as in Ref. [30] for different values of the phases: regions excluded at 95% CL by combining the results of the neutral Higgs boson searches in the whole DELPHI data sample (light-grey). The dashed curves show the median expected limits. The medium-grey areas are the regions not allowed by theory. The CPX scenario corresponds to phases of 90°.

strong suppression of the H_1ZZ coupling due to CP-violation, as already encountered in Fig. 15 in the case of the CPX scenario. More generally [37], the H_1ZZ coupling decreases slowly (by a few tens of %) with phases below about 75° and is strongly suppressed (by three to four orders of magnitude) for phases around 90°. For phases above 100°, the coupling is partially restored, mostly at low $\tan\beta$. This explains the evolution of the upper bound of the experimentally excluded area as a function of phases in Figs. 16 and 17. The changes are moderate for phases up to 60° and significant for the 90° and 135° phases, where the experimental sensitivity relies mainly on the H_2Z process at low $\tan\beta$ and on the H_1H_2 production at large $\tan\beta$, both giving large signals at moderate m_{H_1} only, typically below 60 GeV/c^2 (see Fig. 15).

At the 90° and 135° phases, there are also unexcluded areas at masses lower than 60 GeV/c^2 in the intermediate $\tan\beta$ range, between about 4 and 16. These are related to weakened sensitivities in the H_2Z or H_1H_2 searches. To take the CPX scenario as an example, at masses below 15 GeV/c^2, the dominant final state is the $(H_2 \to H_1H_1)Z$ channel. The lack of experimental searches at LEP2 for such final states with m_{H_1} below the $b\bar{b}$ threshold (see Tab. 1) explains the unexcluded area which is observed at these masses, in agreement with the expected sensitivity. The largest value of CL_s in this region is 52% in the renormalisation group framework and 50% in the Feynman-diagrammatic approach. Still in the CPX scenario, the hole at m_{H_1} around 50 GeV/c^2 arises in the region where the decays $H_2 \to H_1H_1$ and $H_2 \to b\bar{b}$ become approximately equal, leading to a loss of significance of the H_2 signals, as pointed out in Section 6.1 (see Fig. 15). The largest value of CL_s in this region is 17% (expected 4%) in the renormalisation group framework and 37% (expected 11%) in the Feynman-diagrammatic approach. In both frameworks, these CL_s values are observed at $\tan\beta\sim4$, $m_{H_1}\sim50$ GeV/c^2 and $m_{H_2}\sim105/107$ GeV/c^2. The observed exclusion in this region is weaker than expected, which is due to a slight excess of data over the expected background. The value of 1-CL_b at the point of weakest exclusion is indeed 15% (corresponding to a 1.4 sigma deviation) in the renormalisation group framework and 12% (1.5 sigma deviation) in the Feynman-diagrammatic approach. Conversely, the largest deviation in the whole hole has a value of 1-CL_b of 3.3% (2.1 sigma deviation) in the two approaches. This value is observed at $\tan\beta\sim16$, $m_{H_1}\sim45$ GeV/c^2 and $m_{H_2}\sim107$ GeV/c^2 in the renormalisation group framework and $\tan\beta\sim11$, $m_{H_1}\sim52$ GeV/c^2 and $m_{H_2}\sim111$ GeV/c^2 in the Feynman-diagrammatic approach. At this point, the CL_s values are 5.4% (expected 0.1%) and 6.5% (expected 0.2%) in the two frameworks, respectively. The combined LEP data show also deviations in this region [7].

Finally, differences between the two theoretical frameworks are visible mainly at large $\tan\beta$, where the Feynman-diagrammatic calculations predict significantly higher H_1Z residual cross-sections (e.g. a factor about 4 in the CPX scenario for m_{H_1} between 40 and 80 GeV/c^2), leading to a better experimental sensitivity. Differences in the phase dependence of the results are also visible, which are likely to reflect the different phase treatment between the two calculations.

7.2 Dependence on μ and M_{susy}

The excluded regions in the $(m_{H_1}, \tan\beta)$ plane for the CPX scenario and its variants with different values of μ and M_{susy} are presented in Fig. 18 for the renormalization group approach [39] and in Fig. 19 for the Feynman-diagrammatic calculations [30]. In all plots, the common CP-violating phase is 90° and the top mass value is 174.3 GeV/c^2.
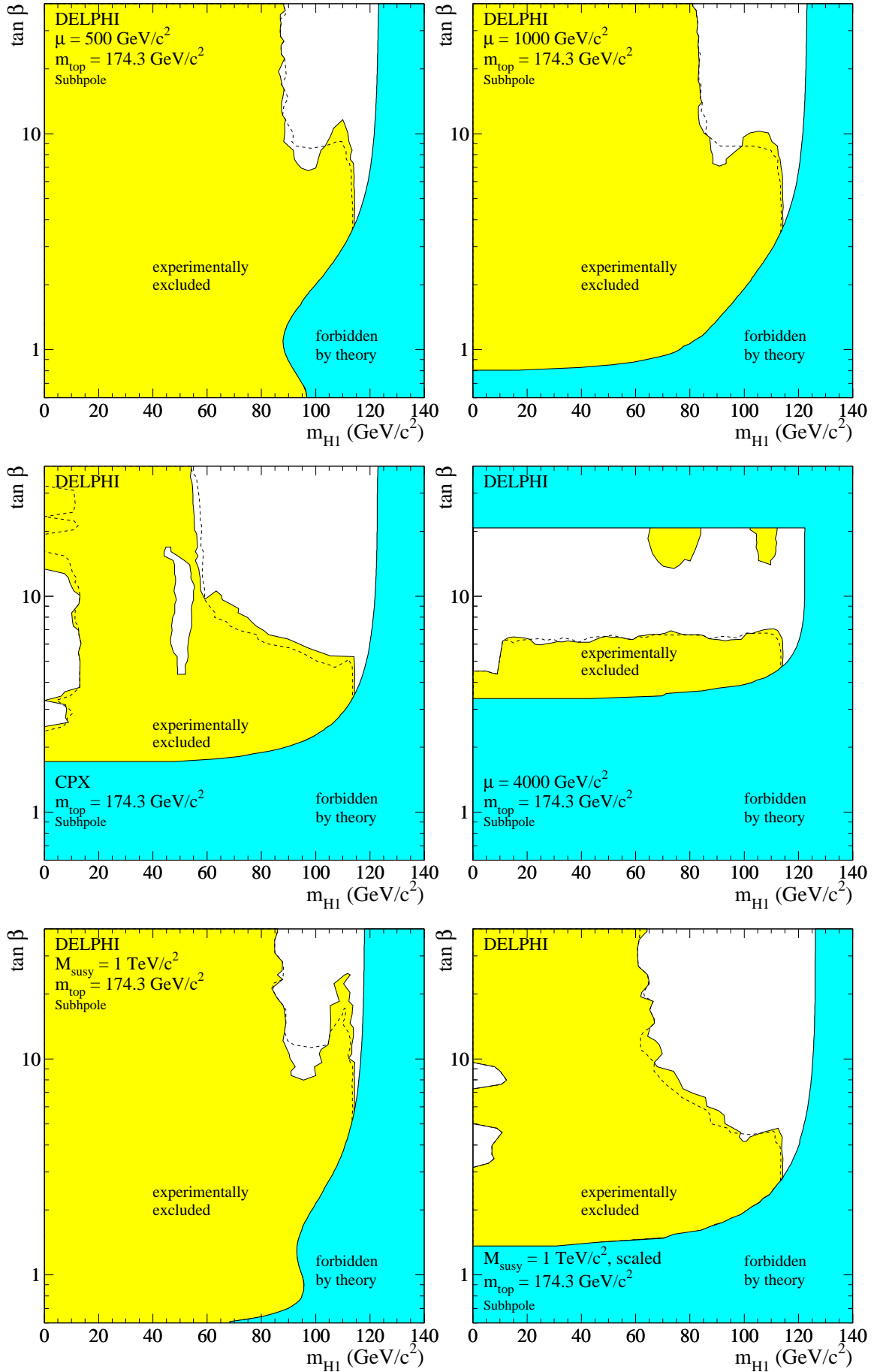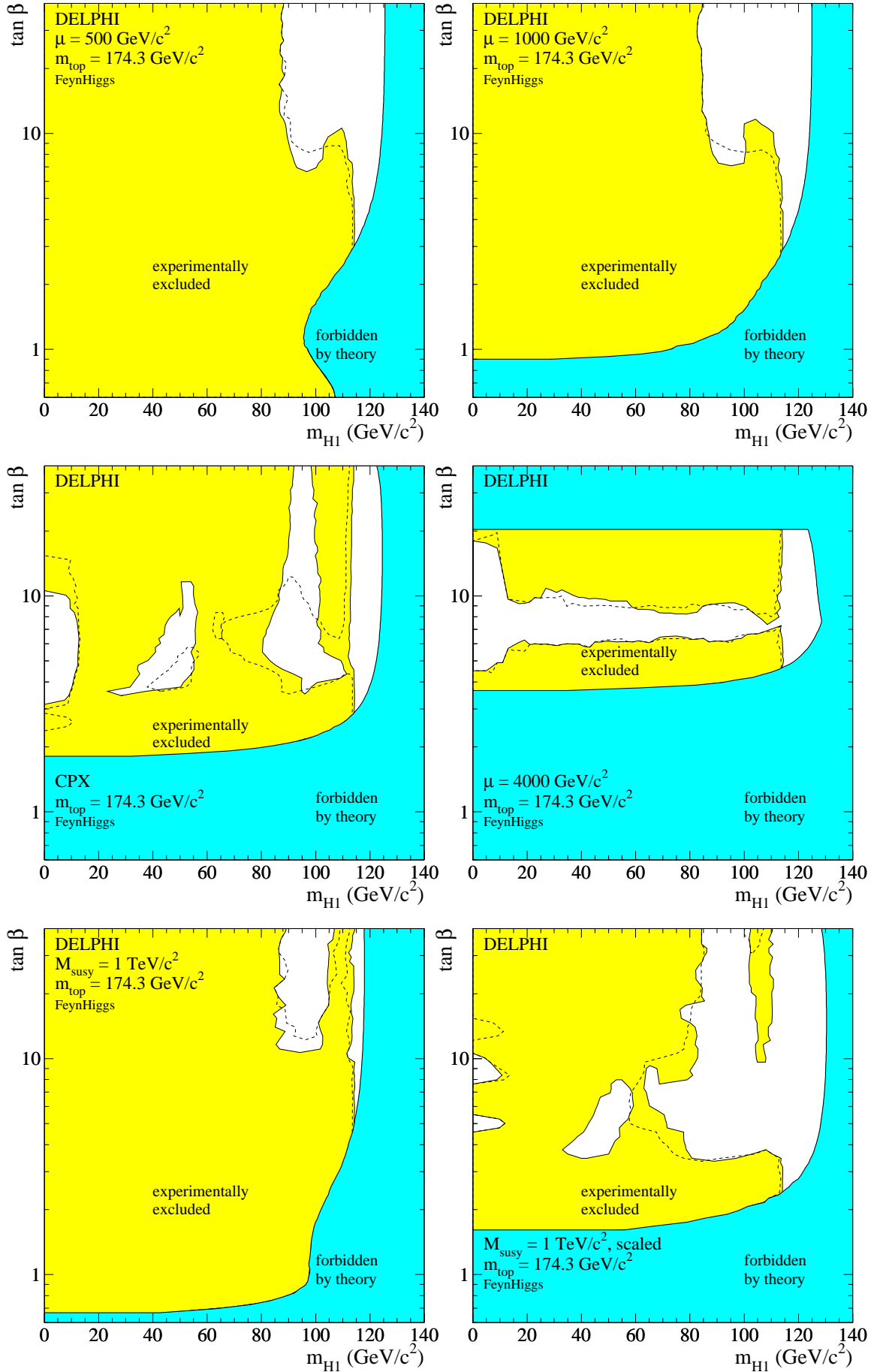
Figure 18: CP-violating MSSM scenarios with corrections as in Ref. [39] for different values of μ and M_{susy}: regions excluded at 95% CL by combining the results of the neutral Higgs boson searches in the whole DELPHI data sample (light-grey). The dashed curves show the median expected limits. The medium-grey areas are the regions not allowed by theory. The CPX scenario corresponds to $\mu = 2000$ GeV/c^2 and $M_{susy} = 500$ GeV/c^2.

Figure 19: CP-violating MSSM scenarios with corrections as in Ref. [30] for different values of μ and M_{susy}: regions excluded at 95% CL by combining the results of the neutral Higgs boson searches in the whole DELPHI data sample (light-grey). The dashed curves show the median expected limits. The medium-grey areas are the regions not allowed by theory. The CPX scenario corresponds to $\mu = 2000$ GeV/c^2 and $M_{susy} = 500$ GeV/c^2.

The dependence of the results on the value of μ is as expected from the scaling of the dominant CP-violating effects with $Im(\mu A)$ (see Section 6.1). The exclusion is almost entirely restored for values of μ lower than 2 TeV/c^2, the value in the CPX scenario, and gets weaker at 4 TeV/c^2. In the first two variants, despite the CP-violating phase being at 90°, there are always two production processes with significant rates in every point of the kinematically accessible parameter space. In the variant at 4 TeV/c^2, due to the large value of μ and the CP-violating phase at 90°, the H_1H_2 and H_2Z processes are suppressed for all values of $\tan\beta$, as well as the H_1Z process at intermediate and large $\tan\beta$ values. In the Feynman-diagrammatic approach, the H_1Z cross-sections are partly restored at large $\tan\beta$ which explains the difference between the results in the two theoretical frameworks in that region. Note also that the theoretically allowed region is much reduced at large $\tan\beta$ in this scenario due to unphysical values of the bottom Yukawa coupling.

The dependence on the value of M_{susy} is presented in the two bottom plots of Figs. 18 and 19. The first scenario corresponds to setting M_{susy} at 1 TeV/c^2, twice its value in the CPX scenario. As the dominant CP-violating effects are proportional to M_{susy}^{-2}, the exclusion is restored in this variant. The reason is as in the case of the two variants with low values of μ, i.e. there are always two production processes with significant rates in every point of the kinematically accessible parameter space. In the second scenario, M_{susy} is still set at 1 TeV/c^2 but the values of $|m_{\tilde{g}}|$, μ and $|A|$ are also scaled by a factor 2, leaving the CP-violating effects almost unchanged (see Section 6.1) with respect to the CPX scenario. This explains why the exclusion region in this variant is close to that in the CPX scenario. The few differences between the excluded regions in these two scenarios are due to different cross-sections for some of the processes which contribute most to the experimental sensitivity, that is the H_1H_2 and H_2Z processes at masses below 60 GeV/c^2, and the H_1Z process at higher masses. As an example, the better coverage of the low mass region at intermediate $\tan\beta$ values in the scaled variant is explained by slightly higher H_1H_2 cross-sections.

7.3   Dependence on m_{top}

The excluded regions in the (m_{H_1}, $\tan\beta$) plane for the CPX scenario with different m_{top} values are presented in Fig. 20 for the renormalization group approach and in Fig. 21 for the Feynman-diagrammatic calculations.

The results show a strong dependence on the value of m_{top}, as expected since the dominant CP-violating effects scale with m_{top}^4. In the two theoretical approaches, the exclusion in the intermediate $\tan\beta$ range is gradually reduced as m_{top} increases and eventually vanishes for $\tan\beta$ between about 3 and 5 and a top mass of 183 GeV/c^2. This can be traced to the suppression of the H_2Z and H_1H_2 cross-sections with increasing values of m_{top}, leaving no significant rate in any of the three possible production channels. At large $\tan\beta$, as m_{top} increases, the H_1H_2 cross-section is reduced and the exclusion gets weaker in the renormalization group approach while it is almost unchanged in the Feynman-diagrammatic framework. As already mentioned, this is a consequence of the higher H_1Z residual cross-sections predicted by the latter calculations at large $\tan\beta$.

7.4   Summary

Scans of the CPX scenario and its variants revealed that CP violation in the Higgs sector can have a significant impact on the experimental sensitivity of LEP. The strong
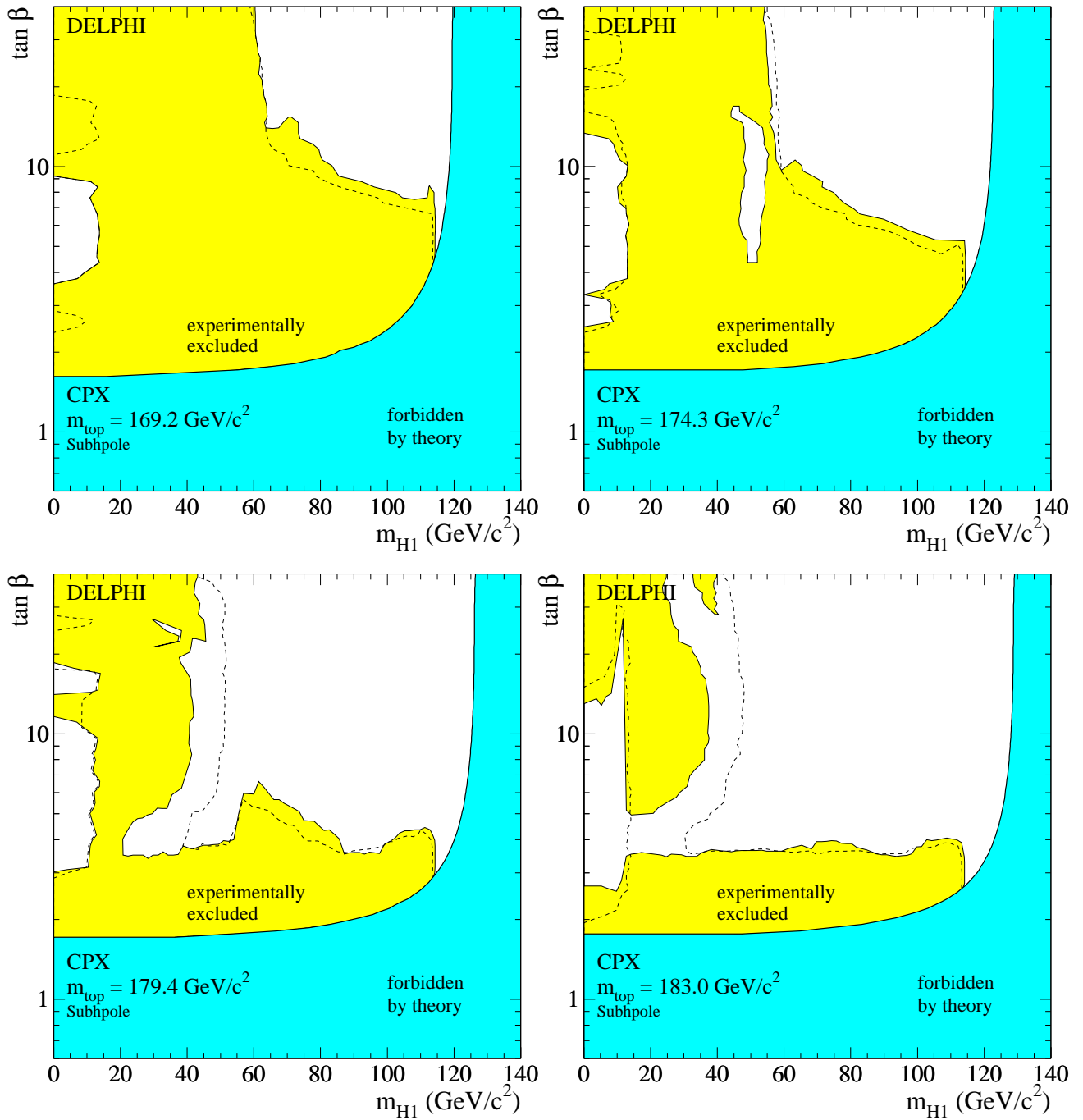
Figure 20: CP-violating MSSM scenarios with corrections as in Ref. [39] for different values of m_{top}: regions excluded at 95% CL by combining the results of the neutral Higgs boson searches in the whole DELPHI data sample (light-grey). The dashed curves show the median expected limits. The medium-grey areas are the regions not allowed by theory.
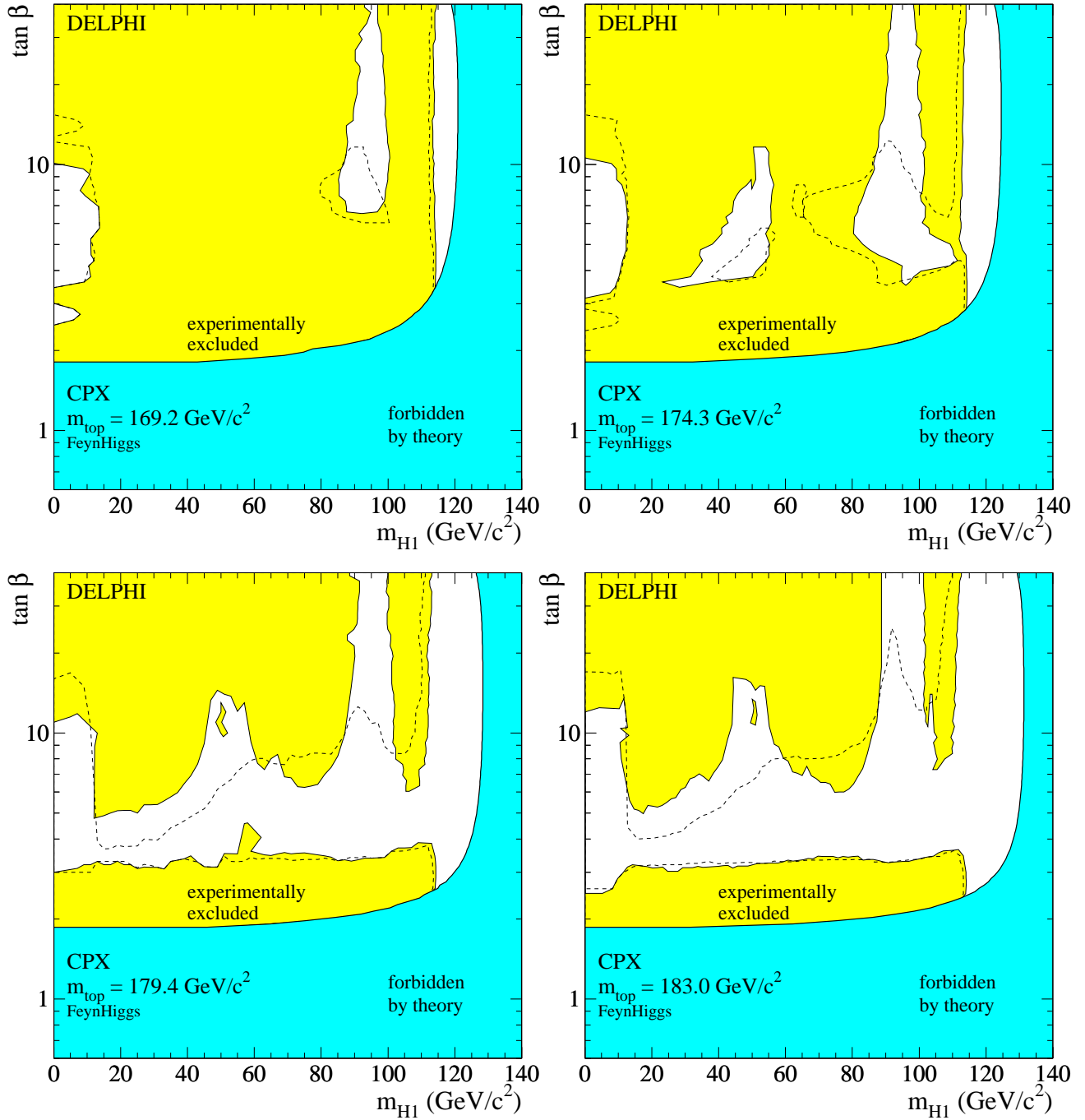
Figure 21: CP-violating MSSM scenarios with corrections as in Ref. [30] for different values of m_{top}: regions excluded at 95% CL by combining the results of the neutral Higgs boson searches in the whole DELPHI data sample (light-grey). The dashed curves show the median expected limits. The medium-grey areas are the regions not allowed by theory.

suppression of the neutral Higgs boson couplings to the Z boson translates into a loss of redundancy in the different search channels, and hence leads to a reduced coverage of the parameter space. The most significant reduction is observed in the intermediate $\tan\beta$ region, typically between 3 and 10, down to the lowest H_1 masses. It occurs for phases between 90° and 135°, top mass values equal to 174.3 GeV/c^2 or larger, and values of the ratio $|\mu A|/M_{susy}^2$ equal to 8 or larger. As a consequence, no absolute mass limits can be derived in these scenarios. On the other hand, the low $\tan\beta$ region appears still disfavoured, as in the CP-conserving models. Scans were performed using two different theoretical approaches for the radiative correction calculations. Although the two sets of results show large differences, they both lead to the same qualitative conclusions.

8 Conclusions

Searches for Higgs bosons in the whole data sample of the DELPHI experiment have been combined to derive constraints on MSSM benchmark scenarios, including models with CP-violation in the Higgs sector. Experimental results encompass searches for neutral Higgs bosons in dominant final states expected in most MSSM models, as well as searches for charged Higgs bosons and for neutral Higgs bosons decaying into hadrons of any flavour, which bring a gain in sensitivity in restricted regions of the parameter space. An additional improvement is obtained by applying the experimental results to more production processes than the two expected main channels, namely the associated production of the lightest Higgs boson with a Z boson and the pair-production of the two lightest Higgs bosons. In the CP-conserving MSSM, the experimental sensitivity at LEP relies on the hZ, hA and HZ channels, the last leading to a significant gain in sensitivity in scenarios where the third neutral Higgs boson, H, is kinematically accessible. In the CP-violating MSSM, the total signal at LEP is spread mainly over the H_1Z, H_2Z and H_1H_2 channels. Accounting for the simultaneous production of all possible signals is essential in this type of scenario where CP-violating effects can lead to strong suppression of one channel or another.

In all CP-conserving scenarios, the experimental results allow a large fraction of the parameter space to be excluded, even in scenarios designed to test potentially difficult cases (e.g. vanishing production cross-sections or decay branching fractions) either at LEP or at hadron colliders. Limits on masses of the h and A bosons were deduced as well as upper and lower exclusion bounds in $\tan\beta$. The dependence of these limits on $m_{\rm top}$ was studied in a range between 169.2 to 183.0 GeV/c^2. To quote but one result, the following limits at 95% of CL have been established in the framework of the $m_{\rm h}^{\rm max}$ scenario with $m_{\rm top} = 174.3$ GeV/c^2:

$m_{\rm h} > 89.7$ GeV/c^2 and $m_{\rm A} > 90.4$ GeV/c^2 for any $\tan\beta$ between 0.4 and 50,
$\tan\beta < 0.72$ or $\tan\beta > 1.96$ for any $m_{\rm A}$ between 0.02 and 1000 GeV/c^2.

These mass limits are insensitive to variations of the top quark mass. The excluded range in $\tan\beta$ decreases with increasing $m_{\rm top}$ and would vanish if $m_{\rm top}$ was as large as 183.0 GeV/c^2. This scenario provides the most conservative bounds on $\tan\beta$ among the eight CP-conserving scenarios tested.

In the CP-violating scenarios, large domains of the kinematically accessible parameter space remain unexcluded due to strong suppressions of the couplings between the Z

and the Higgs bosons induced by CP-violation. Hence no absolute limits can be set on the Higgs boson masses in these scenarios. The unexcluded areas arise in the intermediate $\tan\beta$ range, typically between 3 and 10. Their contours vary considerably with the value of m_{top} and the MSSM parameters which govern the CP-violating effects, $|\mu A|$, M_{susy} and the phase $arg(A)$. These scenarios have been studied in two different theoretical frameworks for the radiative correction calculations. The impact of CP-violation is observed to be qualitatively the same in the two approaches.

Acknowledgements

Appendix 1

We give hereafter efficiencies of the Yukawa $\tau^+\tau^-b\bar{b}$ analysis published in Ref. [21] and applied here to the hA $\rightarrow \tau^+\tau^-q\bar{q}$ signal.

mass (GeV/c^2)		efficiency	mass (GeV/c^2)		efficiency
m_A	m_h	(%)	m_A	m_h	(%)
4	12	0.	12	4	0.
4	20	2.1± 0.3	20	4	1.9±0.3
4	30	2.3± 0.3	30	4	2.0±0.3
4	40	2.6± 0.4	40	4	2.0±0.3
4	50	1.4± 0.3	50	4	1.6±0.3
4	60	1.8± 0.3	60	4	2.2±0.3
4	70	1.3± 0.3	70	4	0.9±0.2
6	12	0.	12	6	0
6	20	2.2± 0.3	20	6	2.0±0.3
6	30	3.1± 0.4	30	6	3.0±0.4
6	40	2.6± 0.4	40	6	2.8±0.4
6	50	2.5± 0.4	50	6	2.2±0.3
6	60	3.1± 0.4	60	6	2.5±0.4
6	70	1.6± 0.3	70	6	1.0±0.2
9	12	0.	12	9	0.
9	20	2.9± 0.4	20	9	2.7±0.4
9	30	3.0± 0.4	30	9	3.4±0.4
9	40	3.4± 0.4	40	9	3.0±0.4
9	50	2.3± 0.4	50	9	2.9±0.4
9	60	2.4± 0.4	60	9	1.8±0.3
9	70	1.1± 0.3	70	9	0.8±0.2
12	12	0.	12	12	0
12	20	2.9± 0.4	20	12	2.6±0.4
12	30	2.3± 0.3	30	12	2.4±0.4
12	40	2.6± 0.4	40	12	2.0±0.3
12	50	2.4± 0.3	50	12	2.4±0.4
12	60	2.0± 0.3	60	12	1.9±0.3
12	70	0.4± 0.2	70	12	0.5±0.2

Table 7: hA $\rightarrow \tau^+\tau^-q\bar{q}$ channel : efficiencies of the selection (in %) at LEP1 as a function of the masses of the A and h bosons. The analysis, described in Ref. [21], was designed to search for Yukawa production in the $\tau^+\tau^-b\bar{b}$ final state. The quoted errors are statistical only.

Appendix 2

We give hereafter efficiencies of the h $\rightarrow$ q$\bar{\text{q}}$ analyses published in Ref. [20,1] and applied to (h $\rightarrow$ AA$\rightarrow$c$\bar{\text{c}}$c$\bar{\text{c}}$)(Z $\rightarrow$ q$\bar{\text{q}}$) signals with low A masses.

m_{A} (GeV/c^2)	m_{h} (GeV/c^2)	Efficiency (%) at 199.6 GeV	Efficiency (%) at 206.5 GeV first period	second period
4.0	10.0	0.6 ± 0.1	0.4 ± 0.1	0.4 ± 0.1
4.0	20.0	1.2 ± 0.1	1.6 ± 0.1	1.4 ± 0.1
4.0	30.0	4.8 ± 0.2	4.9 ± 0.2	4.6 ± 0.2
4.0	50.0	14.4 ± 0.4	15.2 ± 0.4	14.5 ± 0.4
4.0	70.0	13.0 ± 0.4	13.9 ± 0.4	13.5 ± 0.4
4.0	90.0	20.3 ± 0.4	19.3 ± 0.4	18.2 ± 0.4
4.0	105.0	33.1 ± 0.5	27.7 ± 0.5	26.9 ± 0.4
8.0	20.0	1.9 ± 0.1	2.6 ± 0.2	2.3 ± 0.2
8.0	30.0	7.6 ± 0.3	8.3 ± 0.3	7.8 ± 0.3
8.0	50.0	20.9 ± 0.5	21.0 ± 0.4	19.7 ± 0.4
8.0	70.0	20.8 ± 0.4	20.8 ± 0.4	19.8 ± 0.4
8.0	90.0	36.0 ± 0.5	32.8 ± 0.5	31.4 ± 0.5
8.0	105.0	51.6 ± 0.5	44.6 ± 0.5	42.4 ± 0.5

Table 8: (h $\rightarrow$ AA)(Z $\rightarrow$ q$\bar{\text{q}}$) channel with A $\rightarrow$ c$\bar{\text{c}}$: efficiencies of the selection (in %) at $\sqrt{s}$ = 199.6 and 206.5 GeV as a function of the masses of the A and h bosons, for m_{A} between the c$\bar{\text{c}}$ and b$\bar{\text{b}}$ thresholds. Efficiencies at higher masses can be found in Ref. [20,1]. We refer the reader to Ref. [1] for the definition of the two operational periods of the 2000 data taking campaign. The quoted errors are statistical only.

References

[1] DELPHI Collaboration, J. Abdallah et al., Eur. Phys. J. **C32** (2004) 145.

[2] M. Carena and H. Haber, Prog. Part. Nucl. Phys. **50** (2003) 63.

[3] DELPHI Collaboration, J. Abdallah et al., Eur. Phys. J. **C32** (2004) 475;
ALEPH Collaboration, A. Heister et al., Phys. Lett. **B526** (2002) 191;
L3 Collaboration, P. Achard et al., Phys. Lett. **B609** (2005) 35;
OPAL Collaboration, G. Abbiendi et al., CERN-EP-2007-018, submitted to Phys. Lett. B;
ALEPH, DELPHI, L3, OPAL Collaborations and the LEP working group for Higgs boson searches, *Searches for invisible Higgs bosons: preliminary combined results using LEP data collected at energies up to 209 GeV*, LHWG note/2001-06, hep-ex/0107032.

[4] D. E. Groom et al., Eur. Phys. J. **C15** (2000) 1.

[5] The Tevatron electroweak working group for the CDF and D0 collaborations, *A combination of CDF and D0 results on the mass of the top quark*, hep-ex/0703034.

[6] OPAL Collaboration, G. Abbiendi et al., Eur. Phys. J. **C37** (2004) 49.

[7] ALEPH, DELPHI, L3, OPAL Collaborations and the LEP working group for Higgs boson searches, Eur. Phys. J. **C47** (2006) 547.

[8] DELPHI Collaboration, P. Abreu et al., Z. Phys. **C51** (1991) 25.

[9] DELPHI Collaboration, P. Abreu et al., Nucl. Phys. **B342** (1990) 1.

[10] DELPHI Collaboration, P. Abreu et al., Nucl. Phys. **B373** (1992) 3.

[11] DELPHI Collaboration, P. Abreu et al., Nucl. Phys. **B421** (1994) 3.

[12] S. Dagoret, PhD thesis, Université de Paris-Sud, centre d'Orsay, LAL-preprint 91-12 (May 1991).

[13] DELPHI Collaboration, P. Abreu et al., Phys. Lett. **B245** (1990) 276.

[14] DELPHI Collaboration, P. Abreu et al., Z. Phys. **C67** (1995) 69.

[15] DELPHI 92-80 Dallas PHYS 191, *Neutral Higgs Bosons in a Two Doublet Model*, contribution to the 1992 ICHEP conference; quoted by G.Wormser, in proc. of the XXVI ICHEP conference (Dallas, August 1992), Vol. 2, pages 1309-14, ref. 4.

[16] DELPHI Collaboration, W. Adam et al., Z. Phys. **C73** (1996) 1.

[17] DELPHI Collaboration, P. Abreu et al., Eur. Phys. J. **C2** (1998) 1.

[18] DELPHI Collaboration, P. Abreu et al., Eur. Phys. J. **C10** (1999) 563.

[19] DELPHI Collaboration, P. Abreu et al., Eur. Phys. J. **C17** (2000) 187, addendum Eur. Phys. J. **C17** (2000) 549.

[20] DELPHI Collaboration, J. Abdallah et al., Eur. Phys. J. **C23** (2002) 409.

[21] DELPHI Collaboration, J. Abdallah et al., Eur. Phys. J. **C38** (2004) 1.

[22] DELPHI Collaboration, J. Abdallah et al., Eur. Phys. J. **C44** (2005) 147.

[23] DELPHI Collaboration, J. Abdallah et al., Eur. Phys. J. **C34** (2004) 399.

[24] A.L. Read, *Modified Frequentist Analysis of Search Results (The CL$_s$ Method)*, in CERN Report 2000-005, p. 81 (2000), edited by F.James, L.Lyons and Y.Perrin.

[25] R.D. Cousins and V.L. Highland, Nucl. Instr. and Meth. **A320** (1992) 331.

[26] DELPHI 2000-067-PROG-240, *Estimation of probability density functions for the Higgs search*,
http://delphiwww.cern.ch/pubxx/delnote/public/2000_067_prog_240.ps.gz.

[27] A.L. Read, Nucl. Instr. and Meth. **A425** (1999) 357.

[28] S. Heinemeyer, Int. J. Mod. Phys. **A21** (2006) 2659.

[29] M. Carena, S. Heinemeyer, C. Wagner and G. Weiglein, *Suggestions for improved benchmark scenarios for Higgs boson searches at LEP2*, CERN-TH/99-374, DESY

99-186 or hep-ph/9912223;

M. Carena, S. Heinemeyer, C. Wagner and G. Weiglein, Eur. Phys. J. **C26** (2003) 601.

[30] G. Degrassi, S. Heinemeyer, W. Hollik, P. Slavich and G. Weiglein, Eur. Phys. J. **C28** (2003) 133;

see also Ref. [28] and references therein.

[31] S. Heinemeyer, W. Hollik and G. Weiglein, Eur. Phys. J. **C9** (1999) 343.

[32] DELPHI 2003-045-CONF-665, *DELPHI results on neutral Higgs bosons in MSSM benchmark scenarios*, contribution to the 2003 summer conferences, http://delphiwww.cern.ch/pubxx/delnote/public/2003_045_conf_665.ps.gz.

[33] DELPHI 2004-012-CONF-688, *Updated DELPHI results on neutral Higgs bosons in MSSM benchmark scenarios*, contribution to the 2004 summer conferences, http://delphiwww.cern.ch/pubxx/delnote/public/2004_012_conf_688.ps.gz.

[34] A.G. Akeroyd, A. Arhrib and E. Naimi, Eur. Phys. J. **C20** (2001) 51.

[35] DELPHI Collaboration, P. Abreu et al., Eur. Phys. J. **C16** (2000) 371.

[36] DELPHI 2005-020-CONF-740, *Final results from DELPHI on neutral Higgs bosons in MSSM benchmark scenarios*, contribution to the 2005 summer conferences, http://delphiwww.cern.ch/pubxx/delnote/public/2005_020_conf_740.ps.gz.

[37] M. Carena, J. Ellis, A. Pilaftsis, C.E.M. Wagner, Nucl. Phys. **B586** (2000) 92 and Nucl. Phys. **B625** (2002) 345.

[38] M. Carena, J. Ellis, A. Pilaftsis, C.E.M. Wagner, Phys. Lett. **B495** (2000) 155.

[39] M. Carena, M. Quiros and C.E.M. Wagner, Nucl. Phys. **B461** (1996) 407;

H.E. Haber, R. Hempfling and A.H. Hoang, Z. Phys. **C75** (1997) 539;

M. Carena, S. Mrenna and C.E.M. Wagner, Phys. Rev. **D60** (1999) 075010;

see also Ref. [2] and references therein.

[40] J.S. Lee, A. Pilaftsis, M. Carena, S.Y. Choi, M. Drees, J. Ellis and C.E.M. Wagner, Comp. Phys. Comm. **156** (2004) 283.

[41] M. Frank, T. Hahn, S. Heinemeyer, W. Hollik, H. Rzehak and G. Weiglein, J. High Energy Phys. **02** (2007) 047;

S. Heinemeyer, W. Hollik, H. Rzehak and G. Weiglein, *The Higgs sector of the complex MSSM at two-loop order: QCD contributions*, arXiv:0705.0746 [hep-ph].

[42] M. Carena, H.E. Haber, S. Heinemeyer, W. Hollik, C.E.M. Wagner and G. Weiglein, Nucl. Phys. **B580** (2000) 29;

M. Carena, S. Heinemeyer, C.E.M. Wagner and G. Weiglein, Eur. Phys. J. **C45** (2006) 797 (see section 2.1 for a comparison between the two approaches);

see also section 2.4 of Ref. [28].